Master's Thesis – master Water Science and Management

AN EXPERIMENT ON THE EFFECT OF DIFFERENT SLOPES AND INFLOWS ON MANNING ROUGHNESS PARAMETER AT EINIGHAUSEN, SOUTHERN LIMBURG

28 July 2023

Name:	*Osama Alyamoor*	
Student number:	*1315226*	
ECTS:	*30*	
Internship company:	*Sweco Nederland B.V.*	
Supervisors:	*Prof. Dr. Martin Wassen*	*Utrecht University*
	Lucas Nieuweboer	*Sweco Nederland B.V.*
	Roel Bak	*Sweco Nederland B.V.*

Utrecht University

SWECO

Summary

The region of Limburg in the Netherlands experienced heavy rainfall and flooding in 1993, 1995, and 2021. The 2021 flood caused significant damage, with around 2500 houses, 5000 inhabitants, and 600 businesses affected, resulting in a financial loss of €350-600 million. One of the most flooded villages in Southern Limburg is Einighausen, prompting a study by Waterschap Limburg and the municipality of Sittard-Geleen to reduce flooding. The study, conducted by Sweco, uses a hydraulic model and focuses on the Manning roughness parameter, which influences surface runoff. The aim of this research is to incorporate different slopes and different inflows in an experiment to obtain a more accurate Manning's roughness coefficient (n) for the village of Einighausen in Southern Limburg.

To achieve this, an experiment was conducted to investigate the impact of different slopes and inflow rates on the Manning roughness coefficient (n). The experiment involved building a setup with synthetic grass and foam board to mimic impermeable surface conditions. Inflows of 3.5, 4.5, and 5.5 litres per minute (l/min) were tested with slopes ranging from 2° to 20°. Water velocity was measured using a dye tracer, and a 0.6 and 0.7 correction factor were applied for the observed velocities to obtain the mean flow velocity. Using these velocities, Manning roughness coefficients were calculated for various scenarios using the Manning's equation. Linear regression analysis was used to observe different trends in the calculated Manning roughness coefficients. The obtained n values were then modelled in InfoWorks and analysed in QGIS to assess their effects on accumulated water depths in the area.

The results showed that an inflow rate of 3.5 l/min displayed an increase in Manning's roughness coefficient, whereas the other two experiments, 4.5 and 5.5 l/min, displayed a decrease and a slight decrease in Manning's roughness coefficients, respectively, with the latter inflow rate showing more of an equilibrium state. The values of Manning n ranged from 0.015 to 0.147 $s/m^{1/3}$. Furthermore, QGIS-generated difference maps showed higher water depths for Manning's n with a 0.6 factor compared to no factor and 0.7 factor cases.

In conclusion, for slopes ranging from 2° to 20 °, a correction factor of 0.6 should be applied for the observed velocities in combination with higher inflow rates to obtain a more accurate Manning roughness n.

Contents

1. Introduction

Limburg has experienced heavy rainfall and flooding in 1993, 1995 and 2021 (Wind et al., 1999; Wesselink et al., 2013; Delft, 2021). Extreme river discharges have been observed reaching a maximum of 3120 m^3/s and 2861 m^3/s in 1993 and 1995 respectively with 1993 being the most extreme level ever recorded since 1926 (Wind et al., 1999; Wesselink et al., 2013). Estimated flood damages in 1993 and 1995 were around the € 200 and € 125 million respectively (Hoogwater, 2021). The 2021 flood caused an even larger damage; it was estimated that around 2500 houses, 5000 inhabitants and 600 businesses were afflicted by the flood. This translates to a financial loss of € 350 – 600 million compared to current values (Hoogwater, 2021).

One of the most flooded villages in Southern Limburg is Einighausen located in the municipality of Sittard-Geleen (see Figure 1). The village experiences floodings after every heavy rainfall. Therefore, Waterschap Limburg, the water board of Limburg, initiated an exploration study in collaboration with the municipality of Sittard-Geleen to reduce flooding in the area (De Visser, 2023). This exploration is being carried out by Sweco in collaboration with the municipality of Sittard-Geleen, Waterschap Limburg, the residents of Einighausen, farmers, landowners and other stakeholders (De Visser, 2023).

For this study Sweco used a hydraulic model. Important parameters included in the model are infiltration and roughness parameters (De Visser, 2023). Both the infiltration and roughness parameters are used to estimate the surface runoff (Xu et al., 2019). Different slopes and land use yields different infiltration and roughness parameters (Nie et al., 2018; Liu et al., 2003; Zhang et al., 2010) hence a different surface runoff.

The roughness parameter is an important parameter that serves as an indicator for soil erosion and surface runoff because of its influence on the fraction of the soil surface covered by water and overland flow rate (Zheng et al., 2012; Cremers et al., 1996; Zhang et al., 2010; Govers et al., 2000). This parameter is also called the Manning roughness *n* and can be affected by different variables such as vegetation, slopes, and inflow rates of water (Sepaskhah & Bondar, 2002).

This experiment uses different slopes and inflow rates to understand their impact on the Manning roughness parameter. However, little is known about the Manning roughness n in Einighausen as no specific studies have been conducted to investigate how water flows on different surfaces and slopes in this area. Thus, average values are taken for roughness parameters to calculate runoff coefficients leading to inaccurate estimation of runoff. Furthermore, the area consists mainly of grassland. Therefore, synthetic grass is used as a surface to represent grass. However, this study will not take erosion into consideration due to the usage of an impermeable foam layer. Moreover, various studies have been conducted on the effect of infiltration parameters on surface runoff exclusively (Gillies & Smith, 2005; Rawls et al., 1983; Van de Genachte et al., 1996)**.** Thus, infiltration parameter is also excluded in this study. The focus will then be on the effect of different slopes and different inflow rates on the Manning roughness n by using synthetic grass as a surface. Analysing this parameter would be of importance to Waterschap Limburg during extreme rainfall to determine where and how water is flowing, as well as to identify which areas are susceptible to flooding. Furthermore, this study is valuable in determining Manning's roughness coefficient efficiently and cost-effectively across various slopes and inflow conditions.

Therefore, the aim of this study is to incorporate different slopes and different inflows in an experiment to obtain a more accurate Manning's roughness coefficient (n) for the village of Einighausen in Southern Limburg.

This paper has two objectives:

- The first objective is to investigate the effect is of different combinations of slopes and inflow rates on the Manning roughness coefficient *n* for grassland in the village of Einighausen, Southern Limburg, by conducting an experiment.
- The second objective is to analyse what the effects are of the obtained Manning's roughness *n* on inundations by using InfoWorks and QGIS.

The aim and objectives of this study led to the following research question:

> *How can different slopes and different inflows be incorporated in an experiment to obtain a more accurate Manning's roughness n for the village of Einighausen, Southern Limburg?*

And sub-questions:

- What is the effect of different combinations of slopes and inflows on Manning roughness *n* for grassland at the village of Einighausen, Southern Limburg?
- How do the obtained values of Manning roughness *n* affect water depths when applied in InfoWorks and QGIS?

2. Theory

2.1. Manning's Equation

Manning's equation has been the leading method for creating the link between resistance and other variables for a wide range of engineering and scientific applications (Dingman, 2009). Resistance against flow in channels and flood plains is represented with a roughness coefficient (Arcement & Schneider, 1989). This coefficient, also called Manning's roughness coefficient, is one of the key factors for characterizing overland flow (Li & Zhang, 2001). The Manning's equation is used to indirectly calculate the flow velocity (Arcement & Schneider, 1989) and daily peak discharges (Asfaha et al., 2015; Lumbroso & Gaume, 2012).

The Manning's equation is as follows:

$v = \frac{R^{2/3}}{n * S_0^{1/2}}$ with $R_h = \frac{A}{P}$

Where v = flow velocity [m/s], R_h = hydraulic radius [m] and S = slope of channel bed [-], n = roughness coefficient [$s/m^{1/3}$], A = flow area [m^2] and P = wetted perimeter [m] (Abood et al., 2006).

For a rectangular shape A = w * h and P = 2 * h + w where w = wetted width [m] and h = height of water [m]. Therefore, $R = \frac{w * h}{2*h+w}$. However, if the width is a lot larger than the height then R = h.

Thus, $v = \frac{h^{2/3}}{n * S_0^{1/2}}$ in this case.

The Manning's equation is an empirical formula used to analyse uniform flow in open channels. It considers the velocity, flow area, and slope of the channel. In uniform flow conditions, the bottom slope is assumed to be equal to the slopes of the energy grade line and the water surface (NWS, 2023).

2.2. Flow Velocity

Flow velocity is one of the most important parameters to calculate friction coefficients, runoff concentration time and other hydraulic components (Zhang et al., 2010a). Different methods were used to calculate flow velocity for shallow flows such as Acoustic Doppler velocimetry (Gimenez et al., 2004,) particle imaging velocimetry (Ali et al., 2012) and optical tacheometry (Dunkerley, 2003). Acoustic Doppler velocimetry is very useful to measure complicated flow patterns. However, the operating and purchasing costs are high (Bradley et al., 2002). Ali et al. (2012) stated that particle imaging velocimetry can only be utilised in a laboratory setup due to highly developed devices. One of the limitations of optical tacheometry is that it is not applicable in areas were different objects float above water (Dunkerley, 2003). As explained above, these methods show different limitations.

Another widely used technique to measure flow velocities is the dye tracer test (Zhang et al., 2010a; Stern et al., 2001; Otz et al., 2003). Zhang et al. (2010a) measured the travel time of a dye cloud's front from a specific injection point to the end of a given channel. The travelled length was then divided by the observed time to obtain the velocity. Furthermore, a correction factor was applied to the measured surface (V_s) to obtain the mean flow velocity (V). This factor was calculated by the following formula $\alpha_v = V/V_s$.

2.3. Surface Runoff

Surface runoff is the process of water flowing overland towards rivers and eventually into oceans (U.S. Geological Survey, 2019). Water will not be able to infiltrate in the soil and will therefore flow downhill due to gravity. Different aspects affect surface runoff such as rainfall intensity, rainfall amount, rainfall duration, land use, vegetation, soil type, elevation, topography (especially slopes) etc. Hence, different surface-runoff effects would be obtained for different areas (U.S. Geological Survey, 2019).

The Rational Method has been used for more than 150 years to calculate surface runoff (Chin, 2019). This method relates peak runoff with rainfall intensity by the following formula:

$$Q_p = CiA$$

Where Q_p = peak surface runoff [L^3/T], C = runoff coefficient [dimensionless], i = rainfall intensity [L/T] and A = area of the catchment [L^2] (Chin, 2019).

The Rational Method relies on the following assumptions (Chin, 2019; Wang & Wang, 2018; Butler et al., 2018).

1) The rate of rainfall is constant throughout the storm and uniform over the whole catchment.
2) Catchment imperviousness is constant throughout the storm.
3) Contributing impervious area is uniform over the whole catchment.
4) Sewers flow at constant (pipe-full) velocity throughout the time of concentration.

However, these assumptions caused some limitations (Wang & Wang, 2018; Butler et al., 2018). The first and third assumptions would underestimate the results while the second and fourth assumptions overestimate the results (Butler et al., 2018). Furthermore, the Rational Method is used for small catchment areas (Chin, 2019; Butler et al., 2018). However, this method is still widely used for its simplicity (Butler et al., 2018) and for designing stormwater management systems where only peak runoff are of importance (Chin, 2019).

2.4. Modelling

Modelling have been used for different studies (Niet et al., 2014; Etedali et al., 2011; Gilles and Smith, 2015; Mailapalli et al., 2008; Sepaskhah and Bonder, 2002) to obtain the abovementioned n values. The application of various models revealed variations in their performance, with some models performing better as others.

2.5. Used Theories

The Manning's equation and flow velocity methods would be of great importance for the calculation of manning's roughness coefficient. Surface runoff would be of importance for the modelling part of the study and not specifically for the calculation. However, this study used InfoWorks to model inundations and QGIS to analyse the effect of Manning's n on the obtained inundations.

3. Materials and Methods

The theory section led to the following methods. First, an experiment was built to imitate reality. Then, flow velocity was measured. After that, water heights and manning roughness coefficients were calculated and modelled in InfoWorks. Last but not least, the obtained results were analysed using linear regression and QGIS.

3.1. Location

The village of Einighausen lies in the municipality of Sittard-Geleen with coordinates of 51°0’8” N and 5°49’ 33” E (Google Maps, 2023) as shown in the figure below. It has an area of about 307 hectares (Statistieken Buurt Einighausen, 2023). From QGIS different slopes can be seen in Einighausen going up to around 32.57° with elevations ranging from 50 to 61 meters. Several land use can be seen in Einighausen including grassland, agriculture, forest, water, and hard surfaces (pavements, roofs, buildings etc.) (Limburg water board, 2023.

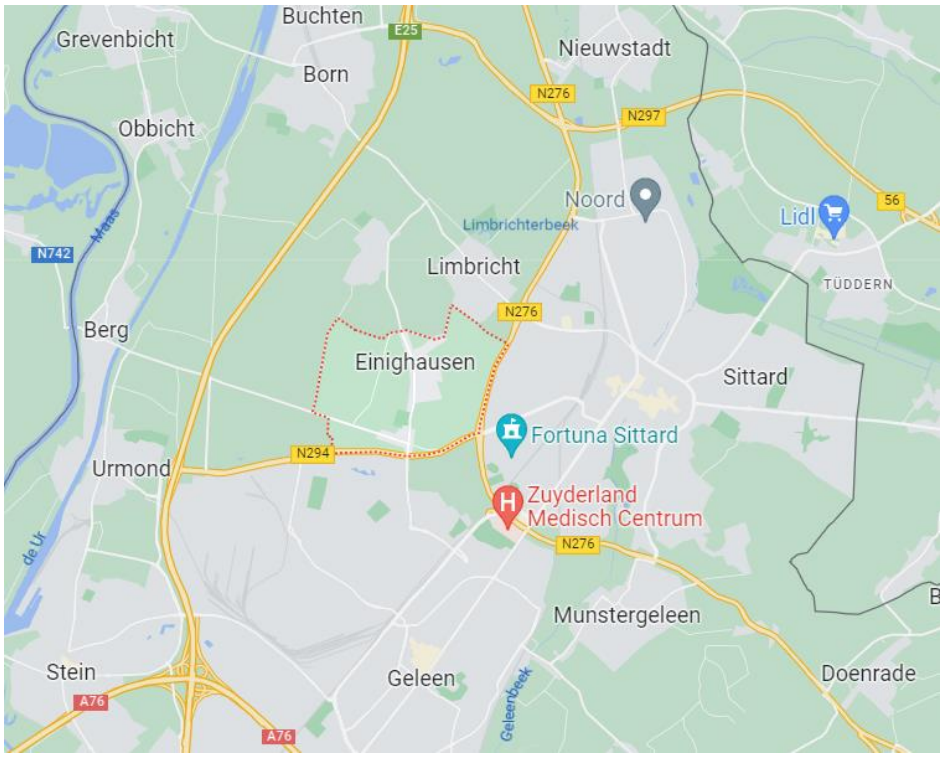

Figure 1 Map of Einighausen, Sothern Limburg. Einighausen is located between Sittard and Geleen. (Google Maps, 2023)

3.2. Data Collection

The slopes of Einighausen were obtained using QGIS. The obtained slopes were used to create the range of slopes for the experimental setup. Water velocity was obtained by timing the water flow on the synthetic grass and dividing the travelled distance by the observed time. Water velocity was used for the calculation of the Manning roughness coefficient. Those steps are further explained in the next sections.

3.3. Experimental setup

The experiment setup was based on the papers of Zheng et al. (2012) and Hessel et al. (2003). Zheng et al. (2012) used boxes of 5m x 1 m x 0.4 m for their experiment. Hessel et al. (2003) used a 2.5 m x 0.4 m plot at a field for the experiment. Hessel et al. (2003) concluded that the roughness parameters (n-values) were not affected by the length of the plot. Both 1 m and 2.5 m lengths provided the same results.
Based on the abovementioned results, the set up was built as follows. Dimensions of 1.45 m x 0.5 m x 0.4 m (Length x Width x Height) were chosen. The end of the setup was left open where water can flow out (see Figure 2).

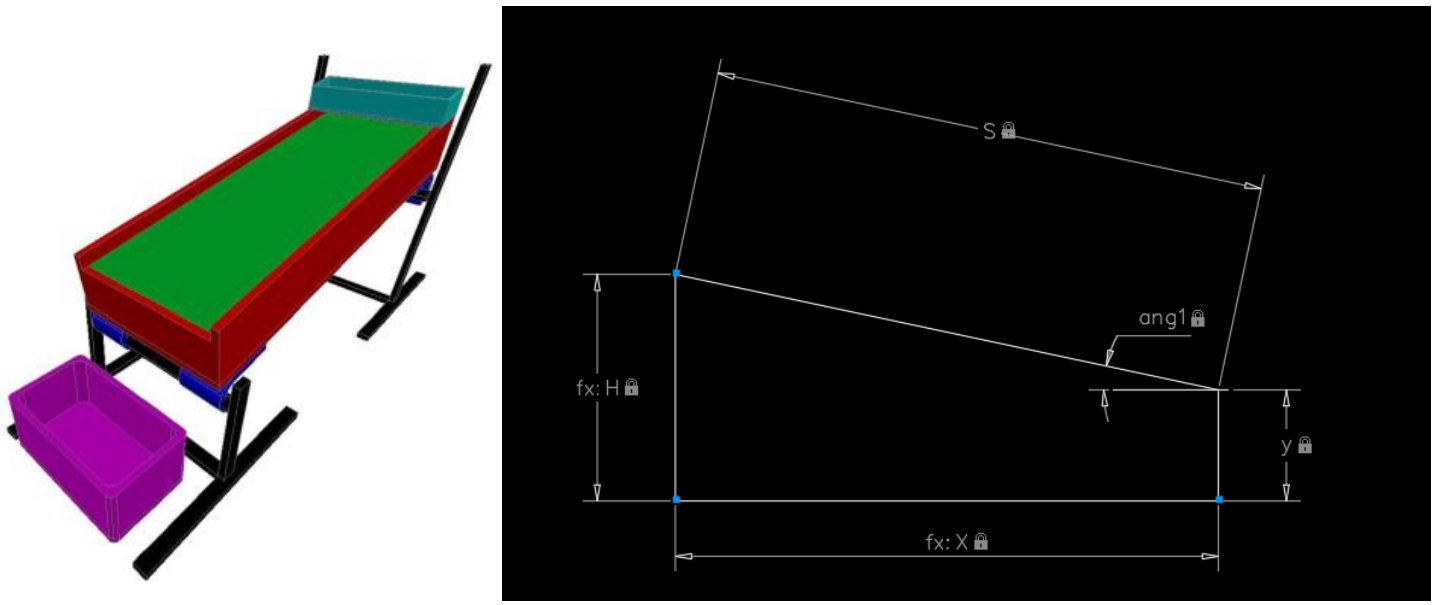

*Figure 2 AutoCAD drawings of the experimental set up. The left figure shows the setup in 3D. The right figure is a side view of the set up with its measurements. H (height) = S*sin(ang1) + y and X = S * cos(ang1) where S = 1.45 m. The angle varies per case hence a different H and X.*

For this experiment infiltration was neglected to focus on the effects of roughness. Therefore, no soil was used as advised by Prof. dr. van Beek. Instead, the surface was sprayed with an impermeable paint, sealed with a plastic cover, and covered with a layer of 0.16 m foam board. This prevents

Figure 3 Experimental setup used for this experiment. A 0.16 m foam board layer was used with a plastic cover on top of it to prevent water seepage on the sides. A layer of synthetic grass was used to mimic grass. For the inflow of water, a perforated tube was built and placed on top of the frame. Furthermore, different slopes were created such that different scenarios can be obtained. The left figure shows the setup at the lowest angle (2°) and the right figure at the highest angle (20°).

water seeping through the wood and prevents water spilling from the sides. Therefore, water will flow directly on the surface. The focus becomes on slopes and inflows. Thus, only roughness will be measured. A layer of foam board of about 0.16 m was laid on top of the surface as mentioned above. This 0.16 m layer consisted of four 0.04 m layers of foam boards. Synthetic grass was used as a top layer (see Figure 3).

To mimic reality the setup was placed on an incline to get a slope. For this experiment slopes of 2°, 5°, 7°, 10°, 12°, 14°, 16°, 18°, 20° were used (see Figure 4). Holes were drilled on both sides of the setup based on the angles used. A rod was used to adjust the angle used for each test.

A few tests were conducted to check if the layer is fully impermeable. The tests showed that water was still seeping from the sides of the experiment and ending up below the foam layer. Therefore, a plastic cover was placed on top of the foam layer to prevent water flowing below the foam layer. Afterwards, the synthetic grass was placed on top of this cover, effectively preventing water from penetrating the foam layer.

Figure 4 Holes were drilled on both sides of the setup based on the angles used. The angles ranged from 2 - 20°. For a better visual representation, the angles were written on the sides. A rod was used to adjust the specified angle of a test.

3.4. Measurements

Constant water flow was achieved by using an inflow meter connected to the tap. Three different inflows were used for this experiment namely 3.5, 4.5, and 5.5 l/min. Higher inflows were not possible due to the limited water pressure in the tap. For an equal distribution of water through the whole area a perforated tube was used. Holes of 2 mm were drilled in the PVC tube (see Figure 5).

Figure 5 A perforated PVC tube was used for the equal distribution of water. 2 mm holes were drilled along the length of the PVC tube. Water will flow into the tube and spread along the holes created.

The next step was to measure the flow velocity. This was based on the method of Zhan et al. (2010a). A dye was poured at the beginning of the experiment at a specific location. After that, the tip of the dye cloud was timed until it reached the end of the experimental setup (see Figure 6). Lastly, the flow velocity was calculated by dividing the travelled distance by the observed time. This process was repeated three times for each scenario. The dye was poured on the left side for the first time, the second time in the middle and the last one at the right side of the experiment.

Figure 6 A dye tracer test was applied to measure the water velocity. First, a specific location was chosen for the placement of the dye. This was marked with a white string taped on the sides as shown in the figure. Then a dye was placed on the specified location. After that, the tip of the dye cloud was measured until it reached the end of the experiment. This process was repeated three times. The dye was first poured on the left side, then in the middle and lastly on the right side.

The average of the three obtained flow velocities were taken as the final value of the velocity for the specified inflow and slope. The experiment was therefore conducted for 81 times (see Table 1). Moreover, the observed velocities were multiplied by the factors 0.7 and 0.6 as suggested in the paper of Zhang et al. (2010a) and by Prof. Dr. Van Beek, respectively. The factor of 0.6 is considered more conservative, as explained by Prof. Dr. Van Beek. Based on the theory of Zhang et al. (2010a) a correction factor was applied to obtain the mean flow velocity.

Table 1 Three inflows and nine slopes were used for this experiment. Furthermore, a dye tracer test was used to observe the velocities. For each combination of slopes and inflows, a dye was placed on three different locations. First on the left side, then in the middle and lastly on the right side. Thus, the experiment was conducted for 81 times.

No.	Land cover	Slopes (°)	Inflow (l/min)	Velocity for different dye locations		
1	Grass	2	5.5	Left	Middle	Right
2	Grass	5	5.5	Left	Middle	Right
3	Grass	7	5.5	Left	Middle	Right
4	Grass	10	5.5	Left	Middle	Right
5	Grass	12	5.5	Left	Middle	Right
6	Grass	14	5.5	Left	Middle	Right
7	Grass	16	5.5	Left	Middle	Right
8	Grass	18	5.5	Left	Middle	Right
9	Grass	20	5.5	Left	Middle	Right
10	Grass	2	4.5	Left	Middle	Right
11	Grass	5	4.5	Left	Middle	Right
12	Grass	7	4.5	Left	Middle	Right
13	Grass	10	4.5	Left	Middle	Right
14	Grass	12	4.5	Left	Middle	Right
15	Grass	14	4.5	Left	Middle	Right
16	Grass	16	4.5	Left	Middle	Right
17	Grass	18	4.5	Left	Middle	Right
18	Grass	20	4.5	Left	Middle	Right
19	Grass	2	3.5	Left	Middle	Right
20	Grass	5	3.5	Left	Middle	Right
21	Grass	7	3.5	Left	Middle	Right
22	Grass	10	3.5	Left	Middle	Right
23	Grass	12	3.5	Left	Middle	Right
24	Grass	14	3.5	Left	Middle	Right
25	Grass	16	3.5	Left	Middle	Right
26	Grass	18	3.5	Left	Middle	Right
27	Grass	20	3.5	Left	Middle	Right

3.5. Calculation

Roughness parameters were calculated by using Manning's equation. In Manning's equation the n-value represents the roughness coefficient. The Manning's equation was rearranged to calculate the roughness coefficient. The following equation was then obtained: $n = \frac{h^{2/3} * S_0^{1/2}}{v}$.

In this case h was unknown. This was obtained by the following equation: Q = v * A where A = w * h and Q = inflow [m^3/s]. The wetted width, velocity and the inflow were known. Rewriting the formula gives the following expression: $h = \frac{Q}{v * w}$. By solving this expression h can be retrieved and the roughness coefficient can now be calculated.

3.6. Analysis

Average values for Manning roughness parameter were calculated and linear regression analysis will be used to find an accurate estimate of n values. Slope was used as a binding component to analyse the relationship between water height (h), velocity (v), and Manning roughness coefficient (n) for the three inflows. Python was used to calculate several statistical values and to create the graph and boxplots.

Furthermore, the obtained *n* values were modelled in InfoWorks and analysed in QGIS to see how they affected the accumulated water on a specific area by measuring the water depth. The obtained Manning roughness coefficients were categorized in four classes namely 2 – 10°, 10 – 16°, 16 – 20° and 20° (see Table 2).

Table 2 The Manning roughness n values were categorized in four classes: 2 – 10°, 10 – 16°, 16 – 20° and 20°. These angles corresponded with the following percentages: 0 – 18 %, 18 – 29 %, 29 – 36 % and >36 %.

nr	Angle (°)	Class (%)
1	2 - 10	0 - 18
2	10 -16	18 -29
3	16 -20	29 - 36
4	20	> 36

Next, the average was taken for the categorized Manning roughness coefficients. Hence, each class had a specific Manning roughness coefficient (last column) that can be used to model surface runoff in InfoWorks (see Table 3).

Table 3 The Manning roughness coefficients were calculated with the velocities with no factor, 0.6 factor and a 0.7 factor. The n values were then placed in the classes mentioned earlier. Finally, the average was taken for each class. Therefore, each class had a specific value that can be used in InfoWorks to model the inundations in Einighausen.

No/0.6/0.7 factor				
Class	**n Exp1**	**n Exp2**	**n Exp3**	**Avg. n**
1	x	x	x	x
2	x	x	x	x
3	x	x	x	x
4	x	x	x	x

Furthermore, difference maps were created using QGIS for 3 areas in Einighausen (see Annex 3.1.2. and 3.2.2.). First, water depths were analysed for each case (current situation, no factor, 0.6 factor, and 0.7 factor case) (see Annex 3.1.1. and 3.2.1.). Then, water depths of the current situation were subtracted from the calculated water depths from each case. The obtained results were used to create the difference maps in QGIS.

Thus, the village of Einighausen was used to analyse the effect of different Manning n values obtained from the experiment using QGIS. This analysis helped identify which Manning n value caused the most or least inundations in the area, aiding in making an informed choice for the appropriate Manning n value.

4. Results

Three experiments were conducted to see the effect of different slopes and different inflows on Manning's roughness coefficients. Results have shown that the first experiment displayed a slight increase in Manning's roughness coefficient, whereas the other two experiments displayed a decrease in Manning's roughness coefficients. Furthermore, QGIS-generated difference maps showed higher water depths for Manning's n with a 0.6 factor compared to a no factor and 0.7 factor case.

4.1. Experiments

For this experiment he velocity, depth of water and Manning's coefficient were plotted against the slope. The figures below show the obtained results obtained from the experiments. Three experiments with different inflows were conducted. Different trends were observed by analysing the plots. These are as follows:

- Experiment 1 had an increase of velocity, a slight decrease in water depth and a slight increase in Manning's roughness n (see Annex 2.1.1. and 2.1.2 and Figure 7).
- Experiment 2 had an increase of velocity, a slight decrease in water depth and a decrease in Manning's roughness n (see Annex 2.2.1. and 2.2.2. and Figure 8).
- Experiment 3 had an increase of velocity, a slight decrease in water depth and a slight decrease in Manning's roughness n (see Annex 2.3.1. and 2.3.2. and Figure 9).

4.1.1. Experiment 1

This experiment utilized various slopes and inflow rates to observe water velocities on synthetic grass through a dye tracer test. The obtained velocities were then used to calculate the water heights and Manning roughness coefficients n.
For the first experiment, an inflow of 3.5 l/min was used with slopes ranging from 2 – 20°. After conducting a dye tracer test, velocities ranging between 0.081 and 0.213 m/s were observed (see Annex 1.1.). Velocities of 0.049–0.128 m/s and 0.057–0.149 m/s were obtained after multiplying the observed velocities by factors of 0.6 and 0.7, respectively (see Annex 1.1.). A linear regression analysis indicated an increasing trend (Annex 2.1.1.).
Water heights of 0.000915 m and 0.002397 m were calculated using the observed velocities. By utilizing the observed velocities multiplied by factors of 0.6 and 0.7, water heights of 0.001525 m – 0.003995m and 0,001307 m – 0,003424 m were calculated, respectively (see Annex 1.1.). Another linear regression analysis revealed a slight decrease in water heights (Annex 2.1.2.).
The obtained velocities and water heights led to the determination of the following Manning roughness coefficients: 0.021 $s/m^{1/3}$ – 0.063 $s/m^{1/3}$ for the observed velocities (Manning Roughness n), 0.048 $s/m^{1/3}$ – 0.147 $s/m^{1/3}$ for velocities with a 0.6 factor (Manning Roughness n*), and 0.037 $s/m^{1/3}$ – 0.114 $s/m^{1/3}$ for velocities with a 0.7 factor (Manning Roughness n+), as shown in the graphs below. The linear regression analysis of the graphs below revealed an increasing trend for the calculated Manning roughness coefficients.

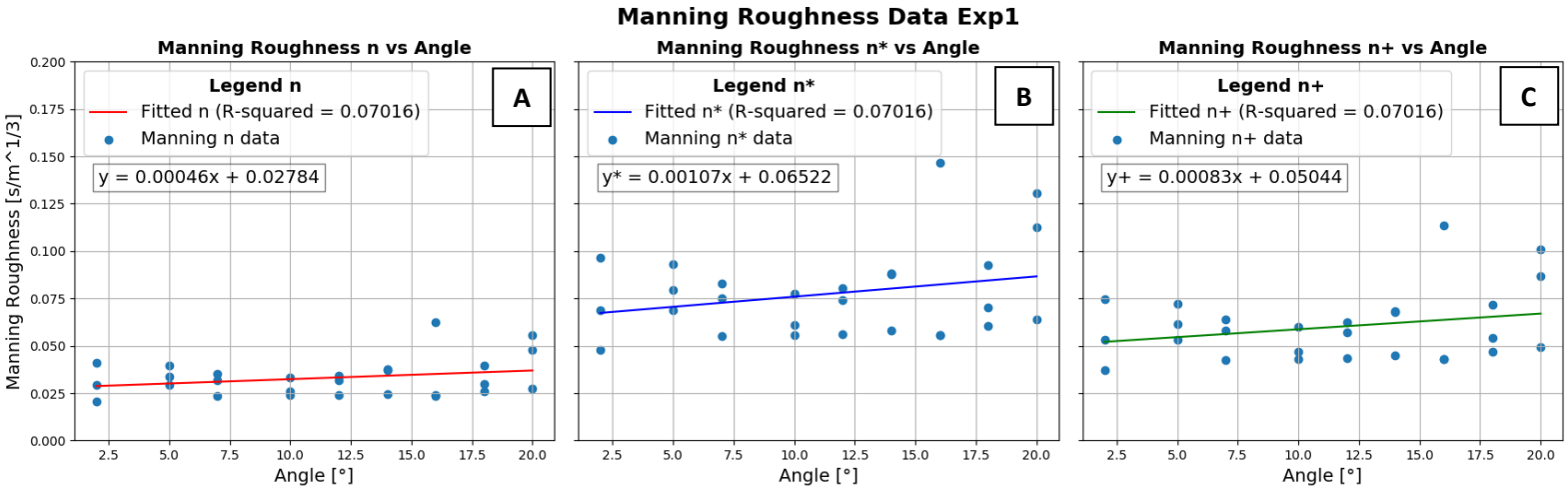

Figure 7 For this experiment an inflow of 3.5 l/min was used with slopes ranging from 2 – 20°. A dye tracer test was used to observe the flow velocity for these conditions. Furthermore, the velocities were multiplied by the correction factors of 0.6 and 0.7. The observed and velocities multiplied by the factors were used to calculate the water heights. The obtained velocities and water heights were utilised to calculate the Manning roughness coefficients. The following ranges of Manning n were calculated: 0.021 s/m$^{1/3}$ – 0.063 s/m$^{1/3}$ for the observed velocities (Figure A), 0.048 s/m$^{1/3}$ – 0.147 s/m$^{1/3}$ for velocities with a 0.6 factor (Figure B), and 0.037 s/m$^{1/3}$ – 0.114 s/m$^{1/3}$ for velocities with a 0.7 factor (Figure C). The three graphs showed an increasing trend.

4.1.2. Experiment 2

This experiment utilized various slopes and inflow rates to observe water velocities on synthetic grass through a dye tracer test. The obtained velocities were then used to calculate the water heights and Manning roughness coefficients n.

For the second experiment, an inflow of 4.5 l/min was used with slopes ranging from 2 – 20°. After conducting a dye tracer test, velocities ranging between 0.064 and 0.262 m/s were observed (see Annex 1.2.). Velocities of 0.038–0.157 m/s and 0.045–0.184 m/s were obtained after multiplying the observed velocities by factors of 0.6 and 0.7, respectively (see Annex 1.2.). A linear regression analysis indicated an increasing trend in water flow velocities (see Annex 2.2.1).

Water heights of 0.000608 m and 0.002510 m were calculated using the observed velocities. By utilizing the observed velocities multiplied by factors of 0.6 and 0.7, water heights of 0.001014 m – 0.004183m and 0.000869 m – 0.003585 m were calculated, respectively (see Annex 1.2.). Another linear regression analysis revealed a slight decrease in water heights (see Annex 2.2.2.).

The obtained velocities and water heights led to the determination of the following Manning roughness coefficients: 0.019 s/m$^{1/3}$ – 0.051 s/m$^{1/3}$ for the observed velocities, 0.044 s/m$^{1/3}$ – 0.119 s/m$^{1/3}$ for velocities with a 0.6 factor, and 0.034 s/m$^{1/3}$ – 0.092 s/m$^{1/3}$ for velocities with a 0.7 factor, as shown in the graphs below. The linear regression analysis of the graphs below revealed a slight decreasing trend for the calculated Manning roughness coefficients.

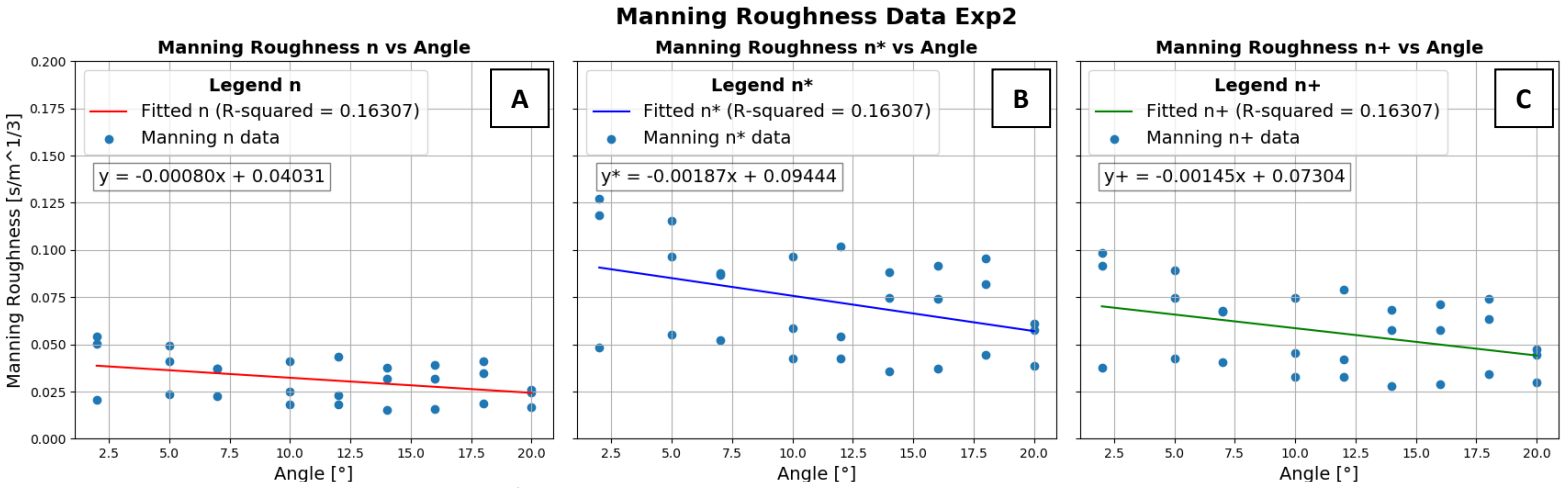

Figure 8 For this experiment an inflow of 4.5 l/min was used with slopes ranging from 2 – 20°. A dye tracer test was used to observe the flow velocity for these conditions. Furthermore, the velocities were multiplied by the correction factors of 0.6 and 0.7. The observed and velocities multiplied by the factors were used to calculate the water heights. The obtained velocities and water heights were utilised to calculate the Manning roughness coefficients. The following ranges of Manning n were calculated: 0.019 $s/m^{1/3}$ – 0.051 $s/m^{1/3}$ for the observed velocities (Figure A), 0.044 $s/m^{1/3}$ – 0.119 $s/m^{1/3}$ for velocities with a 0.6 factor (Figure B), and 0.034 $s/m^{1/3}$ – 0.092 $s/m^{1/3}$ for velocities with a 0.7 factor (Figure C). The three graphs showed a decreasing trend.

4.1.3. Experiment 3

This experiment utilized various slopes and inflow rates to observe water velocities on synthetic grass through a dye tracer test. The obtained velocities were then used to calculate the water heights and Manning roughness coefficients n.

For the third and last experiment, an inflow of 5.5 l/min was used with slopes ranging from 2 – 20°. After conducting a dye tracer test, velocities ranging between 0.071 and 0.207 m/s were observed (see Annex 1.3.). Velocities of 0.042 – 0.124m/s and 0.050 – 0.145 m/s were obtained after multiplying the observed velocities by factors of 0.6 and 0.7, respectively (see Annex 1.3.). A linear regression analysis indicated an increasing trend in water flow velocities (see Annex 2.3.1.).

Water heights of 0.000600 m and 0.001755 m were calculated using the observed velocities. By utilizing the observed velocities multiplied by factors of 0.6 and 0.7, water heights of 0.001001 m – 0.002924 m and 0.000858 m – 0.002507 m were calculated, respectively (see Annex 1.3.). Another linear regression analysis revealed a slight decrease in water heights (see Annex 2.3.2.).

The obtained velocities and water heights led to the determination of the following Manning roughness coefficients: 0.015 $s/m^{1/3}$ – 0.054 $s/m^{1/3}$ for the observed velocities, 0.036 $s/m^{1/3}$ – 0.127 $s/m^{1/3}$ for velocities with a 0.6 factor, and 0.028 $s/m^{1/3}$ – 0.098 $s/m^{1/3}$ for velocities with a 0.7 factor, as shown in the graphs below. The linear regression analysis of the graphs below revealed a decreasing trend for the calculated Manning roughness coefficients.

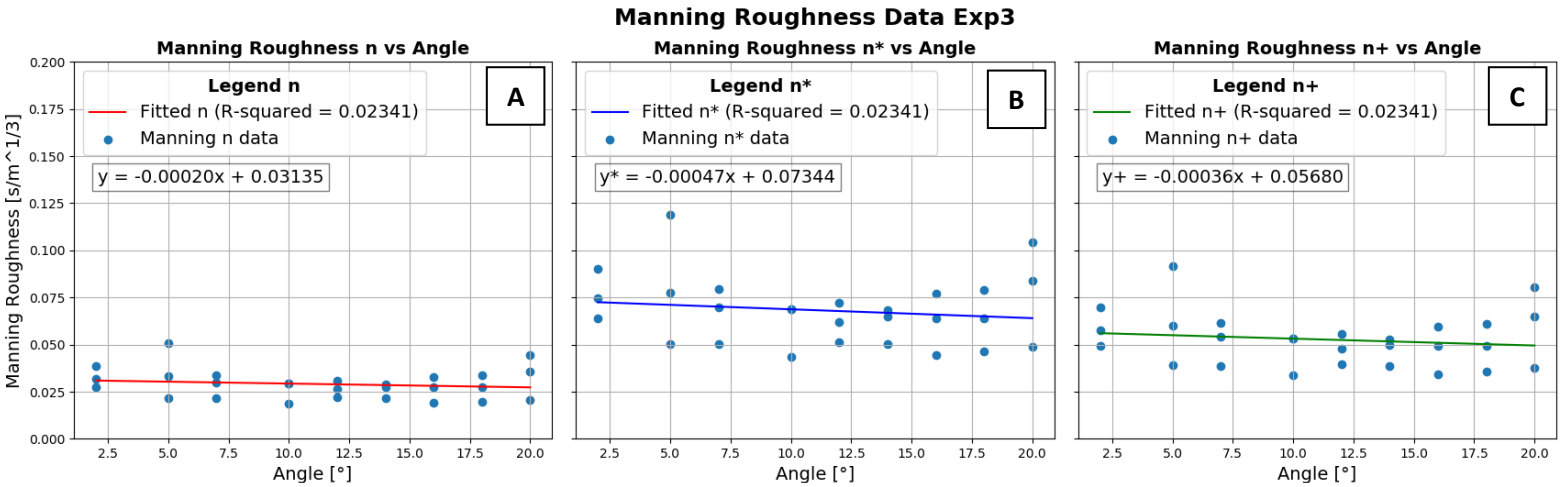

Figure 9 For this experiment an inflow of 5.5 l/min was used with slopes ranging from 2 – 20°. A dye tracer test was used to observe the flow velocity for these conditions. Furthermore, the velocities were multiplied by the correction factors of 0.6 and 0.7. The observed and velocities multiplied by the factors were used to calculate the water heights. The obtained velocities and water heights were utilised to calculate the Manning roughness coefficients. The following ranges of Manning n were calculated: 0.015 $s/m^{1/3}$ – 0.054 $s/m^{1/3}$ for the observed velocities (Figure A), 0.036 $s/m^{1/3}$ – 0.127 $s/m^{1/3}$ for velocities with a 0.6 factor (Figure B), and 0.028 $s/m^{1/3}$ – 0.098 $s/m^{1/3}$ for velocities with a 0.7 factor (Figure C). The three graphs showed a slightly decreasing trend.

4.1.4. Comparison of Manning Roughness n

As explained above, Manning roughness coefficients were calculated using the observed velocities and the velocities multiplied by 0.6 and 0.7 factors. Consequently, boxplots were created based on the obtained Manning roughness coefficients. Below are the boxplots of the Manning roughness coefficients calculated from the observed velocities with no factor (Manning n), velocities multiplied by a 0.6 factor (Manning n*), and velocities multiplied by a 0.7 factor (Manning n+). For the aforementioned cases experiments 1 and 3 had one outlier each as shown in the figure below. Furthermore, the minimum, maximum, mean, median, standard deviation, and standard error were calculated for each experiment (see Annex 2.1.3., 2.2.3. and 2.3.3.). Boxplots have shown that experiment 1 and 3 had one outlier each as can be seen from the figure below. Experiment 1 showed one outlier for each case as shown in the boxplots. The outliers were 0.0626 for Manning n, 0.1468 for Manning n*, and 0.1135 for Manning n+. No outliers were observed from the second experiment as can be seen from the boxplots. The outliers for the third experiment were 0.0507 for Manning n, 0.1187 for Manning n*, and 0.09179 for Manning n+.

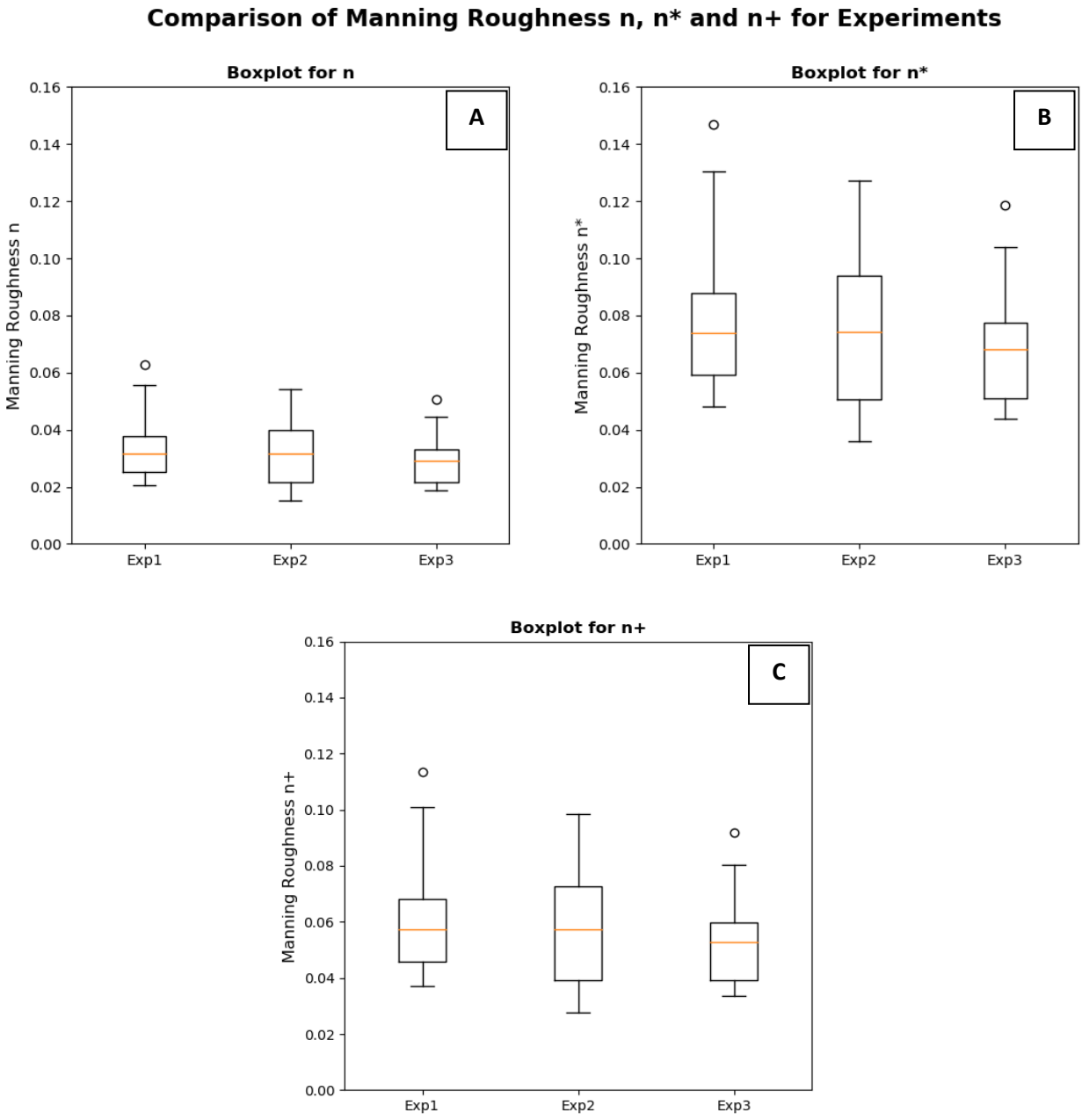

Figure 10 The Manning's n calculated from the observed velocities (Manning n) and velocities multiplied by the factors 0.6 (Manning n) and 0.7 (Manning n+) were used to create a boxplot. Experiments 1 and 3 showed one outlier for each case. The outliers for Experiment 1 were 0.0626 (Figure A), 0.1468 (Figure B), and 0.1135 (Figure C). Experiment 3 showed the following outliers: 0.0507 (Figure A), 0.1187 (Figure B), and 0.09179 (Figure C). No outliers were observed for Experiment 2.*

The tables below present an overview of the calculated statistics for experiment 1, 2 and 3. The calculated statistics include the maximum, minimum, mean, median, standard deviation, and standard error of the calculated Manning n. The values ranged from 0.01534 to 0.14675 $s/m^{1/3}$. The mean and median values showed a consistent similarity across all three experiments. The mean and median values for the three experiments were on average: 0.03 $s/m^{1/3}$ for Manning n, 0.07 $s/m^{1/3}$ for Manning n*, and 0.06 $s/m^{1/3}$ for Manning n+. Experiment 2 exhibited the highest standard deviation of 0.02658, while experiment 3 had the lowest standard deviation of 0.00753. The standard error ranged from 0.00145 to 0.00511.

Table 4 The maximum, minimum, mean, median, standard deviation, and standard error are given for the calculated Manning roughness coefficients of experiment 1. The highest values were found for Manning n whereas Manning n showed the lowest values. The mean and median values had a slight difference to each other. Standard deviations ranged from 0.0099 – 0.02319 for the three cases. The standard errors for Manning n, Manning n*, and Manning n+ were 0.0019, 0.00446, and 0.00345 respectively.*

Exp 1			
	Manning n ($s/m^{1/3}$)	**Manning n* ($s/m^{1/3}$)**	**Manning n+ ($s/m^{1/3}$)**
Minimum	0.02051	0.04804	0.03716
Maximum	0.06264	0.14675	0.1135
Mean	0.03312	0.07759	0.06001
Median	0.0316	0.07403	0.05726
Standard Deviation	0.0099	0.02319	0.01794
Standard Error	0.0019	0.00446	0.00345

Table 5 The maximum, minimum, mean, median, standard deviation, and standard error are given for the calculated Manning roughness coefficients of experiment 2. The highest values were found for Manning n whereas Manning n showed the lowest values. The mean and median values were almost similar each other for Manning n and Manning n+. Standard deviations ranged from 0.01134 – 0.02658 for the three cases. The standard errors for Manning n, Manning n*, and Manning n+ were 0.00218, 0.00511, and 0.00396 respectively.*

Exp 2			
	Manning n ($s/m^{1/3}$)	**Manning n* ($s/m^{1/3}$)**	**Manning n+ ($s/m^{1/3}$)**
Minimum	0.01534	0.03593	0.02779
Maximum	0.05427	0.12715	0.09834
Mean	0.03108	0.07282	0.05632
Median	0.03166	0.07417	0.05736
Standard Deviation	0.01134	0.02658	0.02056
Standard Error	0.00218	0.00511	0.00396

Table 6 The maximum, minimum, mean, median, standard deviation, and standard error are given for the calculated Manning roughness coefficients of experiment 3. The highest values were found for Manning n whereas Manning n showed the lowest values. The mean and median values were almost similar to each other. Standard deviations ranged from 0.00753 – 0.01764 for the three cases. The standard errors for Manning n, Manning n*, and Manning n+ were 0.00145, 0.00339, and 0.00263 respectively.*

Exp 3			
	Manning n ($s/m^{1/3}$)	**Manning n* ($s/m^{1/3}$)**	**Manning n+ ($s/m^{1/3}$)**
Minimum	0.01863	0.04365	0.03376
Maximum	0.05066	0.11868	0.09179
Mean	0.02903	0.068	0.05259
Median	0.02909	0.06815	0.05271
Standard Deviation	0.00753	0.01764	0.01364
Standard Error	0.00145	0.00339	0.00263

4.2. QGIS

For this analysis Manning's n was classified into three groups and water depths were modelled using InfoWorks. Difference maps showed that Manning's roughness coefficients with no factor and 0.7 factor resulted in lower or slightly higher water depths, while a 0.6 factor led to higher depths compared to the current situation (see Figure 11).

4.2.1. Average n values

The average of the Manning roughness coefficients was taken for three different cases namely a case with no factor used for the observed velocity, a case for a 0.6 factor and a case with a 0.7 factor. This resulted in the averages shown in the tables below. The following averages of Manning roughness coefficients were calculated:

- No Factor: 0.03
- 0.6 Factor: 0.07
- 0.7 Factor: 0.06

For the No Factor case the calculated Manning n values ranged 0.02608 to 0.04369. The average values for each class were as follows: 1) 0.03400, 2) 0.02800, 3) 0.03000, and 4) 0.03300 (see Table 7).

For the 0.6 Factor case the calculated Manning n values ranged 0.05251 to 0.10237. The average values for each class were as follows: 1) 0.07900, 2) 0.06600, 3) 0.07100, and 4) 0.07800 (see Table 8).

For the 0.7 Factor case the calculated Manning n values ranged 0.04061 to 0.07917. The average values for each class were as follows: 1) 0.06100, 2) 0.05100, 3) 0.05500, and 4) 0.06000 (see Table 9).

Table 7 The obtained Manning roughness coefficients were categorized in four classes for the No Factor case. This was done for the three experiments. Finally, the average of each class was taken. The averages ranged from 0.028 – 0.034.

No factor				
Class	**n Exp1 ($s/m^{1/3}$)**	**n Exp2 ($s/m^{1/3}$)**	**n Exp3 ($s/m^{1/3}$)**	**Avg. n ($s/m^{1/3}$)**
1	0.03165	0.03737	0.03199	0.03400
2	0.03031	0.02824	0.02608	0.02800
3	0.03423	0.03025	0.02667	0.03000
4	0.04369	0.02241	0.03367	0.03300

Table 8 The obtained Manning roughness coefficients were categorized in four classes for the 0.6 Factor case. This was done for the three experiments. Finally, the average of each class was taken. The averages ranged from 0.066 – 0.079.

Factor of 0.6				
Class	**n factor Exp1 ($s/m^{1/3}$)**	**n factor Exp2 ($s/m^{1/3}$)**	**n factor Exp3 ($s/m^{1/3}$)**	**Avg. n ($s/m^{1/3}$)**
1	0.07416	0.08756	0.07496	0.07900
2	0.07102	0.06615	0.06110	0.06600
3	0.08020	0.07086	0.06248	0.07100
4	0.10237	0.05251	0.07889	0.07800

Table 9 The obtained Manning roughness coefficients were categorized in four classes for the 0.7 Factor case. This was done for the three experiments. Finally, the average of each class was taken. The averages ranged from 0.051 – 0.061.

Factor of 0.7				
Class	**n factor Exp1 ($s/m^{1/3}$)**	**n factor Exp2 ($s/m^{1/3}$)**	**n factor Exp3 ($s/m^{1/3}$)**	**Avg. n ($s/m^{1/3}$)**
1	0.05736	0.06772	0.05797	0.06100
2	0.05493	0.05116	0.04726	0.05100
3	0.06203	0.05481	0.04833	0.05500
4	0.07917	0.04061	0.06101	0.06000

4.2.2. Difference maps

To perform the analysis three areas were chosen with the most water accumulations. This led to the following areas: Area 1, Area 16, and Area 18 (see Figure 11).

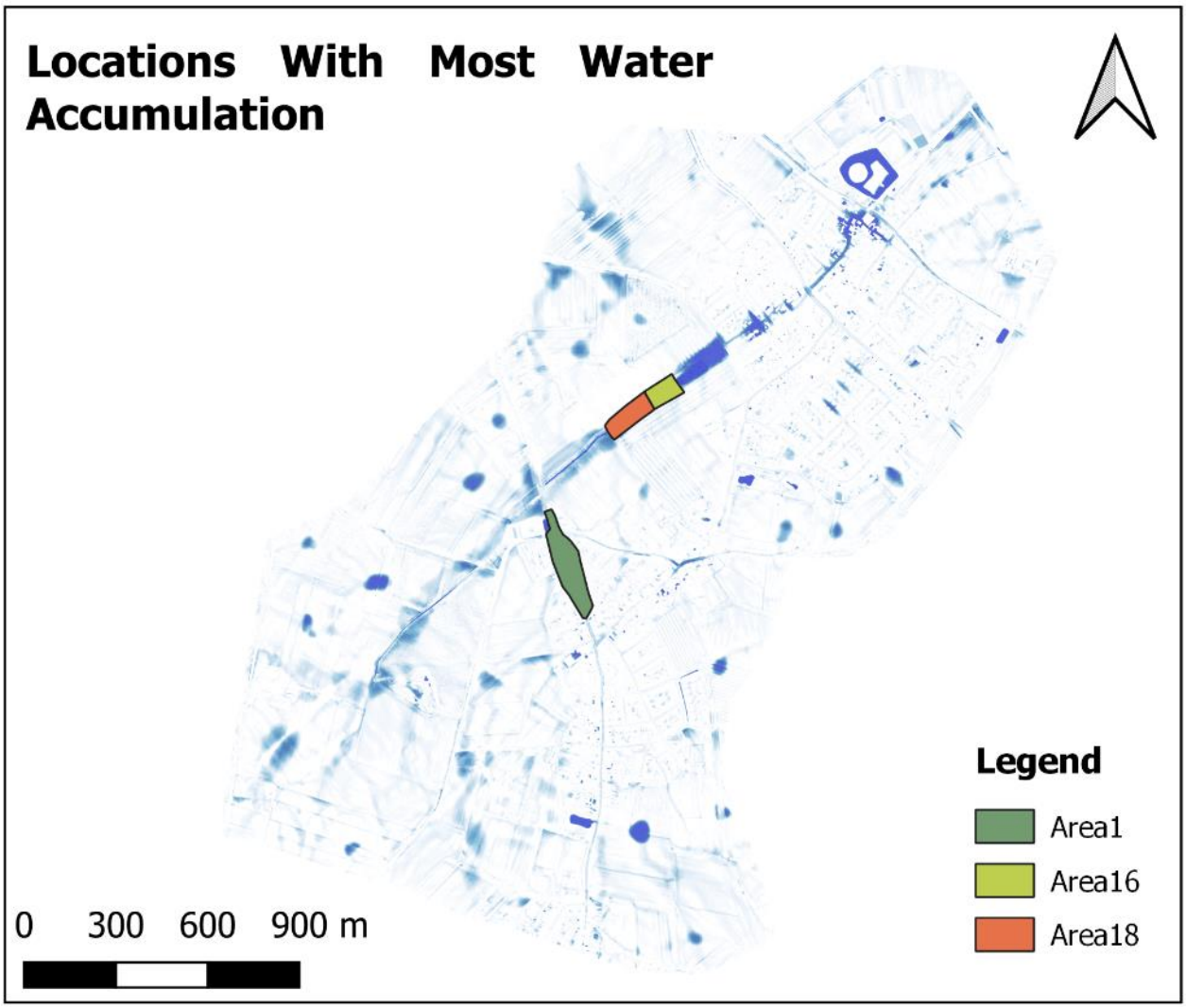

Figure 11 After modelling with InfoWorks, inundated areas were obtained. Three areas with the most water accumulation, namely Area 1, Area 16, and Area 18, were chosen for the analysis.

Difference maps were created for each situation using QGIS. Figure 12 shows the water depth of the current situation, no factor case, 0.6 factor case, and 0.7 factor case. Water depths ranged from 0 – 1.219 m for the current situation and 0 – 1.252 m for the no factor, 0.6 factor, and 0.7 factor case.

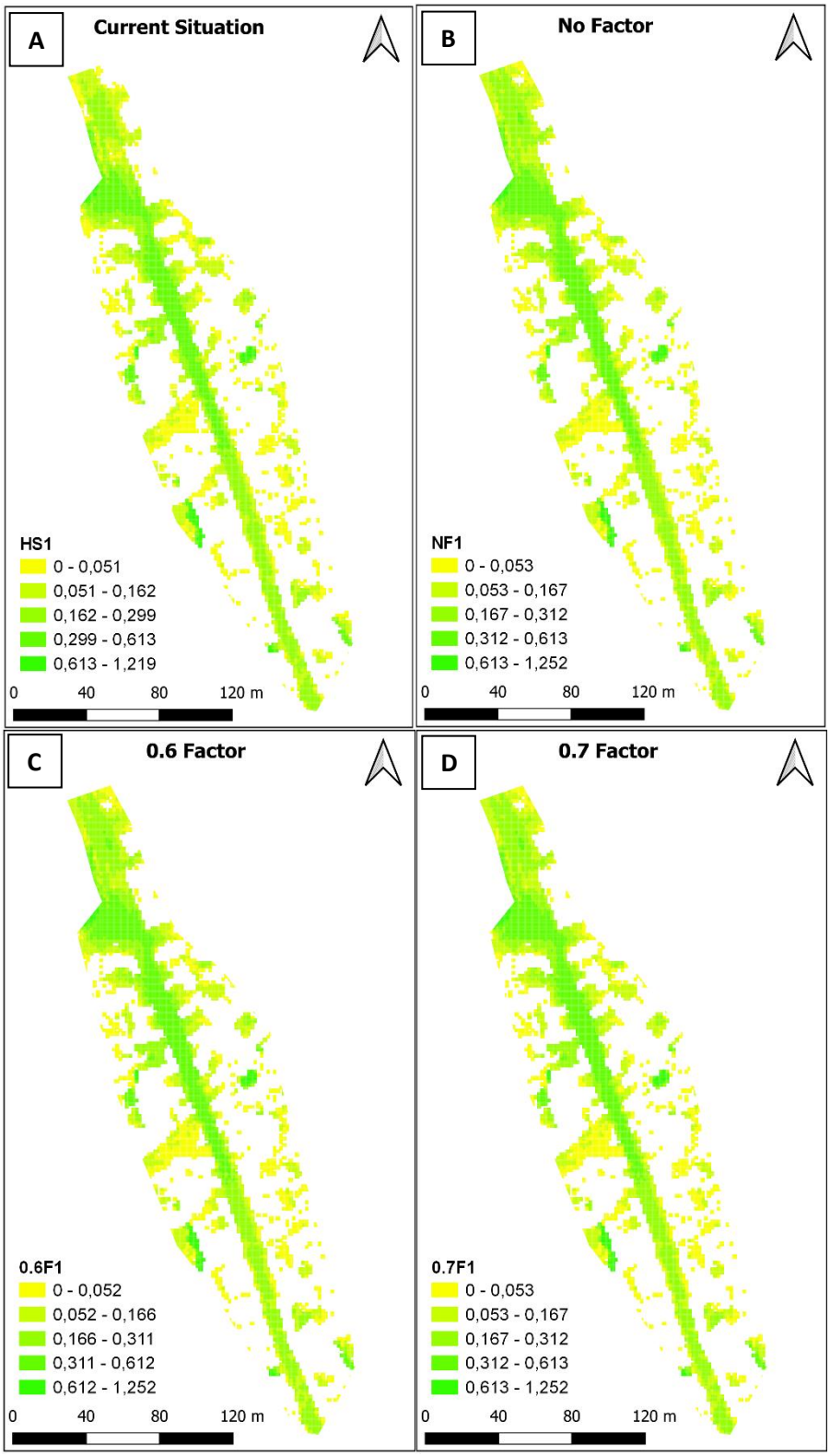

Figure 12 Water depth maps were created using QGIS for the Current Situation, No Factor, 0.6 and 0.7 Factor scenarios. These maps will be used to create the difference maps. The water depth values ranged from 0 to 1.219 m for the Current Situation (Figure A) and 0 to 1.252 m for the No Factor (Figure B), 0.6 Factor (Figure C), and 0.7 Factor case (Figure D).

The provided cases were utilized to generate the difference maps depicted in the figure below. A green or brown colour indicates a higher or slightly higher water depth than the current situation, while red colour indicates lower water depths. The left and middle figures showed similar results whereas the right figure displayed a different pattern. The difference map with a 0.6 factor exhibited a greater prevalence of green colours whereas the other two situations exhibited more red and brown colours.

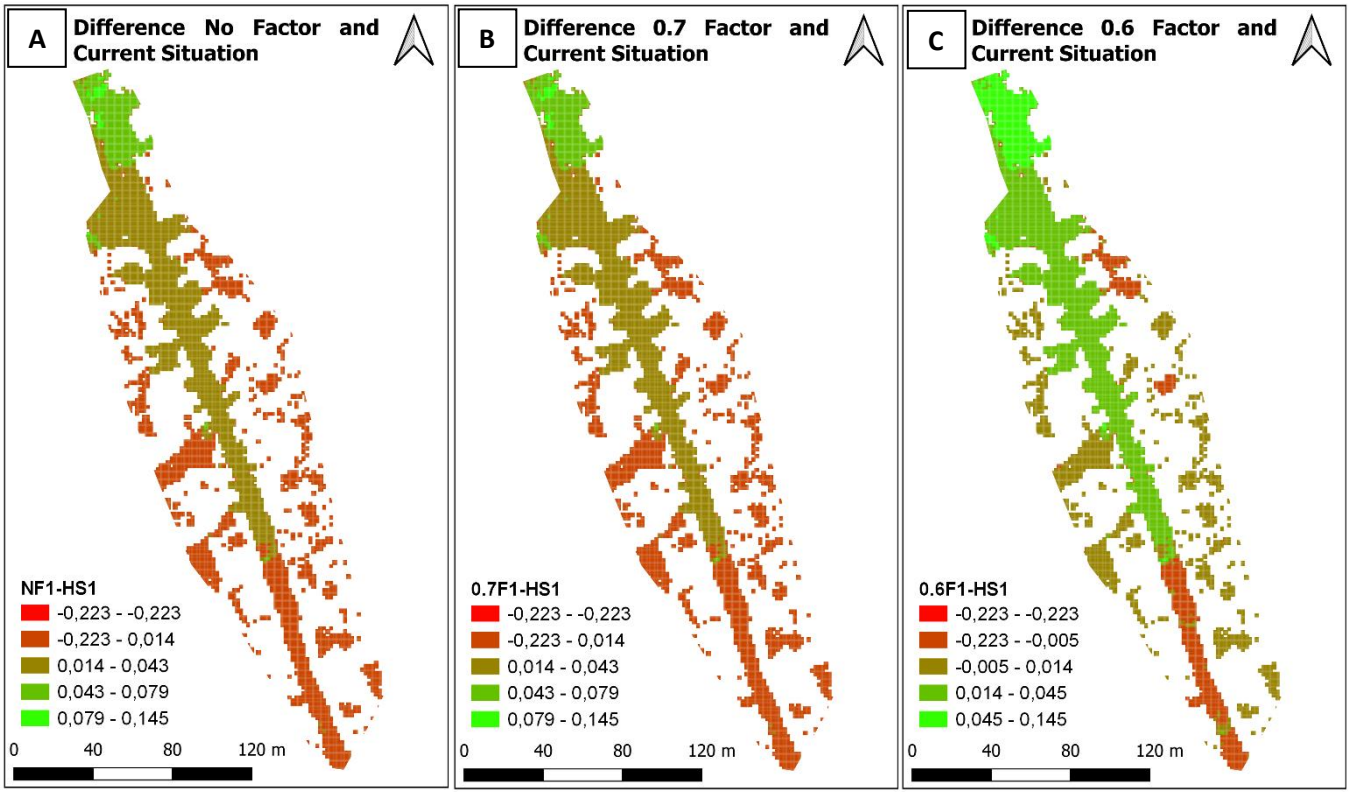

Figure 13 The water depths maps were used to create the difference maps by subtracting the No Factor, 0.6 and 0.7 Factor cases from the Current Situation. The maps showed green, brown, and red colours. A green or brown colour indicates a higher or slightly higher water depth than the current situation, while red colour indicates lower water depths. The No Factor (Figure A) and 0.7 Factor (Figure B) displayed more red and brown colours whereas the 0.6 Factor (Figure C) displayed a greater prevalence of green colours.

5. Discussion

For this study, linear regression, QGIS and statistics were used to analyse the data obtained from the experiment. Linear regression and statistics helped in comparing different Manning n and finding trends. QGIS was used to see how these trends of Manning n affected inundations in Einighausen.

5.1. Evaluation of Results and Reliability Analysis

Different Manning roughness coefficients have been found for different surfaces in the literature. Nortier and De Koning (1991) and Bot (2016) suggested values of 0.025 – 0.035 for straight pathways, pathways with little vegetation, and meadows. Furthermore, Thomsen and Hjalmarson (1991) and Chow (1959) showed similar values for short grass ranging from 0.025 – 0.035.

From the experiments conducted, the mean and median value of Manning n (No Factor) is exactly in the middle of the ranges of the literature. However, Manning roughness coefficients calculated with a factor displayed values approximately double those reported in the literature. Hessel et al. (2003) encountered the same situation. The obtained Manning's n showed a higher value than the data published from different scientific papers. However, this study differed slightly from the study conducted by Hessel et al. (2003). In this study, the presence of an impermeable and non-erodible layer was considered, while the study conducted by Hessel et al. (2003) involved erodible soil. Nevertheless, a similar pattern was observed in both studies. Therefore, the same can be concluded for this study; not including a factor for velocities when calculating Manning's n would result in a more comprehensive and comparable study.

As explained above the following averages of the Manning roughness coefficients were obtained: 0.03 s/m1/3 when no factor is applied, 0.07 s/m1/3 for a 0.6 factor, and 0.06 s/m1/3 for a 0.7 factor. These calculated Manning roughness coefficients were applied in InfoWorks and analysed using QGIS. This helped in visualizing the effects of different Manning coefficients. From the QGIS-generated difference maps it can be observed that a higher value of Manning's n resulted in higher water depths whereas lower Manning's n displayed lower water depths. A higher value of Manning's n indicates greater resistance to the flow of water. Therefore, a higher value of Manning's n would result in greater water retention, leading to greater inundations in specific areas. Conversely, a lower value of Manning's n indicates a lower resistance to the flow of water. Therefore, water flows more easily, resulting in a reduced accumulation of water in specific areas.

Moreover, Sepaskhah and Bonder (2002) evaluated Manning's n for different inflows and slopes. The study was conducted on clay loam soil at different growth stages of wheat and thus different vegetation covers. They concluded that Manning's n varied inversely with inflow and directly with slope. For this study, experiment 1 demonstrated an increasing trend for Manning's n for a lower inflow, while experiments 2 and 3 exhibited a decreasing trend for a higher inflow. Therefore, the obtained results for Manning's n aligned with the findings reported in the literature for the inflow conditions. However, this cannot be said for the slope conditions. Experiments 2 and 3 exhibited a lower Manning's n at an increasing slope. Thus, experiments 2 and 3 did not align with the literature. Mailapalli et al. (2008) discovered that eroded areas resulted in increased shear, leading to higher roughness. In contrast, deposited sediment resulted in a smoother surface, resulting in a decrease in roughness. Therefore, one potential explanation for this case is that the presence of the impermeable layer acted as a smoother surface, resulting in a decrease in roughness and consequently a decrease in Manning's n.

However, in experiment 1, an increase in Manning's n was observed with an increase in slope, aligning with the findings reported in the literature. This increase in Manning's n can be explained by an inaccurate measurement of velocities where the timing of water flow was not precise. Late stoppage or early start of timing can result in lower measured velocities, leading to an increase in Manning's n. Additionally, the placement of the dye during the experiment can also influence Manning's n. A higher placement of the dye introduces an increased distance, which subsequently increases the measured time. Using this observed timing alongside the assigned distance leads to a decrease in velocity, resulting in a higher value of Manning's n.

Outliers were observed for experiments 1 and 3. As mentioned earlier, the accuracy of timing and dye placement plays a critical role in velocity measurements. Inaccuracies in timing and/or dye placement could lead to decreased velocities, consequently resulting in an increase in Manning's n. Additionally, water flows through different pathways, with some tests having longer pathways than others. The longer the pathway, the lower the velocity. Hence, a lower Manning's roughness coefficient. Given the small scale of the experiment, it can be sensitive to minor variations.

By analysing the histograms, it is clear that experiments 1 and 3 are skewed to the right or positively skewed (see Annex 4.1. and 4.3.). The data is concentrated on lower values with a tail extending towards the right side, indicating a great number of lower values compared to higher values. This skewness is caused by outliers obtained in both experiments stretching the curve to the right side. This observation is also supported by the slightly higher mean values compared to the median values. The median leans more towards the lower values due to the longer tail on the right.

However, experiment 2 exhibits more or less a normal distribution (see Annex 4.2.). This suggests that the data is evenly distributed without significant skewness. This observation is further supported by the mean and median values, which are nearly similar.

The standard deviations obtained for experiments 1, 2, and 3 were approximately 29.9%, 36.5%, and 25.9% of the mean values, respectively. Experiment 2 displayed a higher standard deviation, indicating a greater spread or variability in the data. On the other hand, experiment 3 displayed a lower standard deviation, suggesting that the data points were closer to the mean.

The standard error, representing the precision of the mean estimates, was about 5.7%, 7%, and 5% of the mean values for experiments 1, 2, and 3, respectively. These relatively small standard errors indicate that the sample means are more representative of the true means, indicating higher accuracy and reliability in the data.

It can be concluded that the data obtained were accurate and reliable. The values matched the literature, and the obtained low standard errors indicate a high level of precision in the measurements. These reliable results make it possible to find answers to the research questions.

5.2. Management and Policy Implications

The data obtained from the experiment demonstrated relatively low standard errors, indicating a higher level of precision and reliability. Consequently, reliable data can be acquired to analyse the impacts of various inflows and slopes in different regions using a fast and cost-effective method.

The usage of this experiment would greatly benefit policymakers, managers, or consultants by providing them with rapid and dependable results for a specific area. This allows for informed decision-making or the provision of specific advice to clients, based on reliable information.

This experiment can be applied to the village of Einighausen. Specific slopes and inflows can be used to mimic a specific area in Einighausen. Furthermore, synthetic grass would generate similar results to grasslands as explained earlier. Therefore, a fast and affordable way to obtain different Manning roughness coefficients is to use synthetic grass. The most common slopes in Einighausen were between 2 to 14 degrees. This resulted in the following values of Manning's n: 0.05615 for experiment 1, 0.05944 for experiment 2, and 0.05261 for experiment 3. An average of 0.056 was obtained for Einighausen. This falls in the category of Manning n+ which has an average of 0.06. Difference maps have shown that Manning's n+ exhibited a greater prevalence of slightly higher or lower water depths than the current situation. A more precise approach is to take grass (with some soil) samples from a specific area in Einighausen and use it as a surface instead of synthetic grass. This would lead to more accurate results for the area.

Furthermore, this study can be used to explore ways to harness nature for flood mitigation and control. Different types of vegetation would provide varying levels of resistance to water flow, as indicated by their respective Manning n values. Vegetation with higher Manning n values would offer greater resistance, slowing down the flow of water, whereas those with lower Manning n values would provide lower resistance, allowing water to flow more freely. By strategically combining different vegetation types, it becomes possible to influence the flow of water in the desired matter, effectively slowing down or redirecting floods. This way excess water can be redirected to specific areas where it can be stored for later usage.

Moreover, the insights from this study have potential applications in drought management as well. In specific areas, vegetation with higher values can be used to encourage controlled inundation. This approach allows water to permeate the soil slowly, replenishing groundwater reserves during drought periods.

Therefore, it is advised to create tables with Manning roughness coefficients for different vegetation types, categorized into classes based on the slopes found in specific areas. Additionally, the classified Manning coefficients should be analysed to understand their effects on water flow for a specified vegetation type. This approach would save policymakers, managers, and consultants a lot of time and effort providing them with reliable approximations by simply referencing the effects of different Manning n values for specific classes from a standardized table, as demonstrated in the case of Einighausen above. Standardized tables would streamline the process of selecting appropriate Manning n values, facilitating more efficient decision-making and planning for flood control and water resource management.

5.3. Scientific Implications

Typically, field experiments or laboratory experiments are conducted for this type of research. However, this study focused on a fast and cost-effective approach to calculate Manning roughness coefficients. Compared to other experiments, this experiment excluded infiltration by utilizing an impermeable layer, resulting in significant time savings. Additionally, the observed and calculated data exhibited similar results to the existing literature.

The trends observed from the collected data showed that Manning n increased for an inflow of 3.5 l/min, then decreased for a 4.5 l/min inflow, and then started to reach more of an equilibrium state for a 5.5 l/min inflow. Furthermore, the highest inflow showed the lowest standard error. Therefore, it has been showed that higher inflows result in better estimations of Manning n. These findings might bring some new insights into other types of vegetation and might contradict the findings of other studies.

Furthermore, a standardized table was created for the calculated Manning roughness coefficients with their effects analysed. This led to a clear overview of how different slopes and inflows on synthetic grass affect water flow. This helped in visualizing the effects of Manning roughness coefficients. Moreover, this study revealed that focusing on solely the vegetation by using impermeable surfaces would give reliable results.

However, the experiment encountered several limitations that need to be acknowledged. Firstly, a limitation was the low inflow of water. The usage of tap water resulted in the highest inflow obtained being 5.5 l/min. To achieve higher inflows, larger containers could have been used. However, it should be noted that water flow would not be constant due to the decrease in pressure as the water height in the container decreases. While Mariotte bottles could have been an alternative, they were not large enough nor available for this experiment.

Another limitation was the inability to reuse the water due to the dye used to trace the flow. Reusing the water would have led to the presence of dye in subsequent experiments, making it difficult to accurately track the flow. Although a flow velocity meter could have been used to overcome this limitation, it would have been relatively expensive and not aligned with the study's objectives. The same limitation would apply if soil had been used, as the water discolouration would have made it challenging to track the dye.

One of the significant limitations of this study was the constraint of time. Conducting experiments using different surfaces could have provided valuable insights. However, the time required to thoroughly investigate additional surfaces, implement them in the experiment, document the process, and evaluate the results would exceed the planned timeframe for this research.

Furthermore, no literature was available specifically focusing on experiments excluding infiltration through the use of an impermeable layer and experiments conducted on synthetic grass. Additionally, access to literature on experiments related to grassland was also restricted, further limiting the available resources for comparison and analysis. As a result, alternative literature sources were utilized to complement the findings and compare the obtained results.

Future studies can expand on this experiment. Research can be conducted on different surfaces such as soil, vegetation, and/or pebbles/stones. This step requires a thorough investigation of the aforementioned surfaces. When using soil, erosion will play a role. Therefore, for each step soil height should be checked to make sure that the soil is not washed away completely. Additionally, measurement of flow velocity would be challenging. A flow velocity meter would be relatively expensive. A cheaper option would be fluorescent dyes. This type of dye can be visible in water that has discolouration.

Moreover, when using vegetation and pebbles/stones, density plays an important role. It is advised to start experimenting with high densities i.e., 80% density and slowly going to lower densities. The lower limit is reached when similar results are obtained for a specified density with bare areas. Additionally, diameters and distances for these surfaces are important. Hereby, scaling plays a critical role. Literature on scaling vegetation and pebbles/stones should be thoroughly investigated.

Finally, it is important to consider using higher inflows during the experimentation process to obtain a clear effect on Manning roughness coefficients. Higher inflows can be achieved by utilizing a water pump, which ensures a constant and controlled water flow rate. By employing higher inflows, the experiment can simulate more realistic and challenging conditions, providing valuable data on the behaviour of Manning roughness coefficients under varying flow rates.

6. Conclusion

The aim and objectives of this study led to the following research question:

> *How can different slopes and different inflows be incorporated in an experiment to obtain a more accurate Manning's roughness n for the village of Einighausen, Southern Limburg?*

And sub-questions:

- What is the effect of different combinations of slopes and inflows on Manning roughness *n* for grassland at the village of Einighausen, Southern Limburg?
- How do the obtained values of Manning roughness *n* affect water depths when applied in InfoWorks and QGIS?

Experimental data has shown that higher inflow rates for slopes ranging from 2 – 20 ° resulted in a more equilibrium state whereas lower inflow rates exhibited a clear increasing or decreasing trend. Furthermore, difference maps showed that Manning's roughness coefficients with no factor and 0.7 factor resulted in lower or slightly higher water depths, while a 0.6 factor led to higher depths compared to the current situation. Thus, a 0.6 factor led to greater inundations.

It can be concluded that for slopes ranging from 2° to 20 °, a correction factor of 0.6 should be applied for the observed velocities in combination with higher inflow rates to obtain a more accurate Manning roughness n.

Reference list

Abood, M. M., Yusuf, B., Mohammed, T. A., & Ghazali, A. H. (2006). Manning roughness coefficient for grass-lined channel. Journal of Science and Technology, 13(4), 317-330.

Ali, M., Sterk, G., Seeger, M., & Stroosnijder, L. (2012). Effect of flow discharge and median grain size on mean flow velocity under overland flow. Journal of Hydrology, 452, 150-160.

Arcement, G. J., & Schneider, V. R. (1989). Guide for selecting Manning's roughness coefficients for natural channels and flood plains.

Asfaha, T. G., Frankl, A., Haile, M., Zenebe, A., & Nyssen, J. (2015). Determinants of peak discharge in steep mountain catchments–Case of the Rift Valley escarpment of Northern Ethiopia. Journal of Hydrology, 529, 1725-1739.

Bot, B. B. (2016). Grondwaterzakboekje Gwz2016. Bot Raadgevend Ingenieur.

Butler, D., Digman, C. J., Makropoulos, C., & Davies, J. W. (2018). Urban drainage. Crc Press.

Chin, D. A. (2019). Estimating peak runoff rates using the rational method. Journal of irrigation and drainage engineering, 145(6), 04019006.

Chow, V. T. (1959). Open Channel Hydraulics. McGraw-Hill, New York, 680 pp.

Cremers, N. H. D. T., Van Dijk, P. M., De Roo, A. P. J., & Verzandvoort, M. A. (1996). Spatial and temporal variability of soil surface roughness and the application in hydrological and soil erosion modelling. Hydrological processes, 10(8), 1035-1047.

De Visser, J. (2023). Watersysteemanalyse Einighausen: Limburg. Sweco Nederland B.V.

Dingman, S. L. (2009). Fluvial hydraulics. oxford university press.

Dunkerley, D. L. (2003). An optical tachometer for short-path measurement of flow speeds in shallow overland flows: improved alternative to dye timing. Earth Surface Processes and Landforms: The Journal of the British Geomorphological Research Group, 28(7), 777-786.

Etedali, H. R., Ebrahimian, H., Abbasi, F., & Liaghat, A. (2011). Evaluating models for the estimation of furrow irrigation infiltration and roughness. Spanish Journal of Agricultural Research, 9(2), 641-649.

Gillies, M. H., & Smith, R. J. (2005). Infiltration parameters from surface irrigation advance and run-off data. Irrigation Science, 24, 25-35.

Gillies, M. H., & Smith, R. J. (2015). SISCO: surface irrigation simulation, calibration and optimisation. Irrigation science, 33, 339-355.

Giménez, R., Planchon, O., Silvera, N., & Govers, G. (2004). Longitudinal velocity patterns and bed morphology interaction in a rill. Earth Surface Processes and Landforms: The Journal of the British Geomorphological Research Group, 29(1), 105-114.

Google Maps (n.d.).[Village of Einighausen, Southern Limburg, The Netherlands]. Retrieved March 10, 2023, from https://www.google.com/maps/place/Einighausen/@50.9977947,5.8263964,12.33z/data=!4m6!3m5!1s0x47c0c7a5a193c9a1:0x58fb08ccdd2d73cb!8m2!3d51.0022236!4d5.8266196!16s%2Fg%2F122y5qt4?hl=nl

Govers, G., Takken, I., & Helming, K. (2000). Soil roughness and overland flow. Agronomie, 20(2), 131-146.

Hessel, R., Jetten, V., & Guanghui, Z. (2003). Estimating Manning's n for steep slopes. Catena, 54(1-2), 77-91.

Hoogwater, T. F. F. F. (2021). Hoogwater 2021 Feiten en Duiding. ENW report.

Li, Z., & Zhang, J. (2001). Calculation of field Manning's roughness coefficient. Agricultural water management, 49(2), 153-161.

Limburg water board. (2023).

Liu, G., Xu, M., & Ritsema, C. (2003). A study of soil surface characteristics in a small watershed in the hilly, gullied area on the Chinese Loess Plateau. Catena, 54(1-2), 31-44.

Lumbroso, D., & Gaume, E. (2012). Reducing the uncertainty in indirect estimates of extreme flash flood discharges. Journal of hydrology, 414, 16-30.

Mailapalli, D. R., Raghuwanshi, N. S., Singh, R., Schmitz, G. H., & Lennartz, F. (2008). Spatial and temporal variation of Manning's roughness coefficient in furrow irrigation. Journal of irrigation and drainage engineering, 134(2), 185-192.

Nie, W. B., Fei, L. J., & Ma, X. Y. (2014). Applied closed-end furrow irrigation optimized design based on field and simulated advance data.

Nie, W. B., Li, Y. B., Zhang, F., Dong, S. X., Wang, H., & Ma, X. Y. (2018). A method for determining the discharge of closed-end furrow irrigation based on the representative value of Manning's roughness and field mean infiltration parameters estimated using the PTF at regional scale. Water, 10(12), 1825.

Nortier, J. W., & De Koning, P. (1991). Toegepaste vloeistofmechanica; hydraulica voor waterbouwkundigen. Educaboek.

NWS. (2023, July 9). National Weather Service. Opgehaald van https://www.weather.gov/aprfc/NormalDepthCalc#:~:text=The%20Mannings%20equation%20is%20an,flow%20area%20and%20channel%20slope.&text=Under%20the%20assumption%20of%20uniform,and%20the%20water%20surface%20slope.

Otz, M. H., Otz, H. K., Otz, I., & Siegel, D. I. (2003). Surface water/groundwater interaction in the Piora aquifer, Switzerland: evidence from dye tracing tests. Hydrogeology Journal, 11, 228-239.

QGIS Development Team, 2023. QGIS Geographic Information System. Open Source Geospatial Foundation. URL http://qgis.org

Rawls, W. J., Brakensiek, D. L., & Miller, N. (1983). Green-Ampt infiltration parameters from soils data. Journal of hydraulic engineering, 109(1), 62-70.

Sepaskhah, A. R., & Bondar, H. (2002). Sw—soil and water: estimation of manning roughness coefficient for bare and vegetated furrow irrigation. Biosystems Engineering, 82(3), 351-357.

Statistieken Buurt Einighausen . (2023, October 4). Opgehaald van AlleCijfers.nl: Buurt Einighausen (gemeente Sittard-Geleen) in cijfers en grafieken (update 2023!) | AlleCijfers.nl. (2023, October 4). AlleCijfers.nl. https://allecijfers.nl/buurt/einighausen-sittard-geleen/

Stern, D. A., Khanbilvardi, R., Alair, J. C., & Richardson, W. (2001). Description of flow through a natural wetland using dye tracer tests. Ecological Engineering, 18(2), 173-184.

Thomsen, B. W., & Hjalmarson, H. W. (1991). Estimated Manning's roughness coefficients for stream channels and flood plains in Maricopa County. Arizona: Phoenix, Arizona, Flood Control District of Maricopa County.

U.S. Geological Survey. (2019, 8 September) |Surface Runoff and the Water Cycle. https://www.usgs.gov/special-topics/water-science-school/science/surface-runoff-and-water-cycle#:~:text=Last%20page%20Last%20%C2%BB,Overview,of%20the%20natural%20water%20cycle.

Van de Genachte, G., Mallants, D., Ramos, J., Deckers, J. A., & Feyen, J. (1996). Estimating infiltration parameters from basic soil properties. Hydrological Processes, 10(5), 687-701.

Wang, S., & Wang, H. (2018). Extending the Rational Method for assessing and developing sustainable urban drainage systems. Water research, 144, 112-125.

Wesselink, A., Warner, J., & Kok, M. (2013). You gain some funding, you lose some freedom: The ironies of flood protection in Limburg (The Netherlands). Environmental science & policy, 30, 113-125.

Wind, H. G., Nierop, T. M., De Blois, C. J., & de Kok, J. L. (1999). Analysis of flood damages from the 1993 and 1995 Meuse floods. Water resources research, 35(11), 3459-3465.

Xu, J., Cai, H., Saddique, Q., Wang, X., Li, L., Ma, C., & Lu, Y. (2019). Evaluation and optimization of border irrigation in different irrigation seasons based on temporal variation of infiltration and roughness. Agricultural Water Management, 214, 64-77.

Zhang, G. H., Luo, R. T., Cao, Y., Shen, R. C., & Zhang, X. C. (2010a). Correction factor to dye-measured flow velocity under varying water and sediment discharges. Journal of hydrology, 389(1-2), 205-213.

Zhang, G. H., Luo, R. T., Cao, Y., Shen, R. C., & Zhang, X. C. (2010). Impacts of sediment load on Manning coefficient in supercritical shallow flow on steep slopes. Hydrological Processes, 24(26), 3909-3914.

Zheng, Z. C., He, S. Q., & Wu, F. Q. (2012). Relationship between soil surface roughness and hydraulic roughness coefficient on sloping farmland. Water Science and Engineering, 5(2), 191-20

Acknowledgements

I would like to express my heartfelt gratitude to Professor Martin Wassen and Dr. Stefanie Lutz for their critical feedback. I am thankful to my internship supervisors, Roel Bak and Lucas Nieuweboer, for their constant support. My parents' help in building the experiment is deeply appreciated. Lastly, I extend thanks to all who contributed to this research, as it wouldn't have been possible without them. Their guidance, encouragement, and support have shaped this work significantly, making a lasting impact on both the thesis and my personal growth.

Annexes

Annex 1. Measurements

Annex 1.1. Experiment 1

Nr	Angle (°)	Slope(%)	Slope (-)	Dye position	Time (s)	Length (cm)	Velocity (cm/s)	Velocity with factor (cm/s)	Inflow (cm^3/s)	b (cm)
1	0	0	0,000000	Left	23,04	117	5,08	3,05	91,67	47
2	0	0	0,000000	Middle	75,12	117	1,56	0,93	91,67	47
3	0	0	0,000000	Right	83,04	117	1,41	0,85	91,67	47
4	2	3	0,034921	Left	9,47	117	12,35	7,41	91,67	47
5	2	3	0,034921	Middle	14,38	117	8,14	4,88	91,67	47
6	2	3	0,034921	Right	11,77	117	9,94	5,96	91,67	47
7	5	9	0,087489	Left	8,91	117	13,13	7,88	91,67	47
8	5	9	0,087489	Middle	10,7	117	10,93	6,56	91,67	47
9	5	9	0,087489	Right	9,71	117	12,05	7,23	91,67	47
10	7	12	0,122785	Left	7,04	117	16,62	9,97	91,67	47
11	7	12	0,122785	Middle	9	117	13,00	7,80	91,67	47
12	7	12	0,122785	Right	8,49	117	13,78	8,27	91,67	47
13	10	18	0,176327	Left	6,72	117	17,41	10,45	91,67	47
14	10	18	0,176327	Middle	7,76	117	15,08	9,05	91,67	47
15	10	18	0,176327	Right	6,38	117	18,34	11,00	91,67	47
16	12	21	0,212557	Left	6,06	117	19,31	11,58	91,67	47
17	12	21	0,212557	Middle	7,51	117	15,58	9,35	91,67	47
18	12	21	0,212557	Right	7,14	117	16,39	9,83	91,67	47
19	14	25	0,249328	Left	5,88	117	19,90	11,94	91,67	47
20	14	25	0,249328	Middle	7,53	117	15,54	9,32	91,67	47

21	14	25	0,249328	Right	7,57	117	15,46	9,27	91,67	47
22	16	29	0,286745	Left	5,49	117	21,31	12,79	91,67	47
23	16	29	0,286745	Middle	9,84	117	11,89	7,13	91,67	47
24	16	29	0,286745	Right	5,51	117	21,23	12,74	91,67	47
25	18	32	0,324920	Left	5,57	117	21,01	12,60	91,67	47
26	18	32	0,324920	Middle	7,19	117	16,27	9,76	91,67	47
27	18	32	0,324920	Right	6,08	117	19,24	11,55	91,67	47
28	20	36	0,363970	Left	7,81	117	14,98	8,99	91,67	47
29	20	36	0,363970	Middle	8,54	117	13,70	8,22	91,67	47
30	20	36	0,363970	Right	5,57	117	21,01	12,60	91,67	47

h (cm)	h with factor (cm)	n (s/cm^1/3)	n with factor (s/cm^1/3)		h (m)	h with factor (m)	n (s/m^1/3)	n with factor (s/m^1/3)	Average n	Average n with factor
0,38407	0,64012									
1,25223	2,08705									
1,38425	2,30709									
0,15786	0,26310	0,00442	0,01035		0,00158	0,00263	0,02051	0,04804		
0,23971	0,39952	0,00886	0,02076		0,00240	0,00400	0,04114	0,09638		
0,19620	0,32700	0,00635	0,01487		0,00196	0,00327	0,02946	0,06903		
0,14853	0,24755	0,00632	0,01480		0,00149	0,00248	0,02932	0,06870		
0,17837	0,29728	0,00857	0,02008		0,00178	0,00297	0,03978	0,09321	0,03165	0,07416
0,16186	0,26977	0,00729	0,01708		0,00162	0,00270	0,03384	0,07928		
0,11735	0,19559	0,00505	0,01184		0,00117	0,00196	0,02346	0,05496		
0,15003	0,25005	0,00761	0,01783		0,00150	0,00250	0,03532	0,08276		
0,14153	0,23588	0,00691	0,01618		0,00142	0,00236	0,03205	0,07509		
0,11202	0,18670	0,00560	0,01313		0,00112	0,00187	0,02601	0,06095	0,03031	0,07102
0,12936	0,21559	0,00712	0,01669		0,00129	0,00216	0,03306	0,07747		

0,10635	0,17725	0,00514	0,01204		0,00106	0,00177	0,02386	0,05590		
0,10102	0,16836	0,00518	0,01213		0,00101	0,00168	0,02404	0,05633		
0,12519	0,20865	0,00741	0,01735		0,00125	0,00209	0,03437	0,08053		
0,11902	0,19837	0,00681	0,01595		0,00119	0,00198	0,03160	0,07403		
0,09802	0,16336	0,00533	0,01250		0,00098	0,00163	0,02476	0,05801		
0,12552	0,20920	0,00806	0,01888		0,00126	0,00209	0,03739	0,08761		
0,12619	0,21032	0,00813	0,01904		0,00126	0,00210	0,03773	0,08839		
0,09152	0,15253	0,00510	0,01195		0,00092	0,00153	0,02368	0,05549	0,03423	0,08020
0,16403	0,27338	0,01349	0,03162		0,00164	0,00273	0,06264	0,14675		
0,09185	0,15308	0,00513	0,01203		0,00092	0,00153	0,02383	0,05583		
0,09285	0,15475	0,00556	0,01304		0,00093	0,00155	0,02583	0,06051		
0,11986	0,19976	0,00852	0,01995		0,00120	0,00200	0,03952	0,09260		
0,10135	0,16892	0,00644	0,01509		0,00101	0,00169	0,02989	0,07002		
0,13019	0,21698	0,01034	0,02424		0,00130	0,00217	0,04802	0,11249	0,04369	0,10237
0,14236	0,23727	0,01201	0,02813		0,00142	0,00237	0,05573	0,13056		
0,09285	0,15475	0,00589	0,01380		0,00093	0,00155	0,02734	0,06404		

Annex 1.2. Experiment 2

Nr	Angle (°)	Slope (%)	Slope (-)	Dye position	Time (s)	Length (cm)	Velocity (cm/s)	Velocity with factor (cm/s)	Inflow (cm^3/s)	b (cm)
1	0	0	0,000000	Left	29,19	117	4,01	2,40	75,00	47
2	0	0	0,000000	Middle	45,25	117	2,59	1,55	75,00	47
3	0	0	0,000000	Right	42,91	117	2,73	1,64	75,00	47
4	2	3	0,034921	Left	10,33	117	11,33	6,80	75,00	47
5	2	3	0,034921	Middle	17,61	117	6,64	3,99	75,00	47
6	2	3	0,034921	Right	18,4	117	6,36	3,82	75,00	47
7	5	9	0,087489	Left	8,47	117	13,81	8,29	75,00	47

8	5	9	0,087489	Middle	13,18	117	8,88	5,33	75,00	47
9	5	9	0,087489	Right	11,83	117	9,89	5,93	75,00	47
10	7	12	0,122785	Left	7,42	117	15,77	9,46	75,00	47
11	7	12	0,122785	Middle	10,05	117	11,64	6,99	75,00	47
12	7	12	0,122785	Right	10,09	117	11,60	6,96	75,00	47
13	10	18	0,176327	Left	5,88	117	19,90	11,94	75,00	47
14	10	18	0,176327	Middle	7,11	117	16,46	9,87	75,00	47
15	10	18	0,176327	Right	9,58	117	12,21	7,33	75,00	47
16	12	21	0,212557	Left	5,56	117	21,04	12,63	75,00	47
17	12	21	0,212557	Middle	6,43	117	18,20	10,92	75,00	47
18	12	21	0,212557	Right	9,38	117	12,47	7,48	75,00	47
19	14	25	0,249328	Left	4,78	117	24,48	14,69	75,00	47
20	14	25	0,249328	Middle	7,4	117	15,81	9,49	75,00	47
21	14	25	0,249328	Right	8,2	117	14,27	8,56	75,00	47
22	16	29	0,286745	Left	4,67	117	25,05	15,03	75,00	47
23	16	29	0,286745	Middle	7,08	117	16,53	9,92	75,00	47
24	16	29	0,286745	Right	8,05	117	14,53	8,72	75,00	47
25	18	32	0,324920	Left	5,01	117	23,35	14,01	75,00	47
26	18	32	0,324920	Middle	7,24	117	16,16	9,70	75,00	47
27	18	32	0,324920	Right	7,95	117	14,72	8,83	75,00	47
28	20	36	0,363970	Left	4,46	117	26,23	15,74	75,00	47
29	20	36	0,363970	Middle	5,67	117	20,63	12,38	75,00	47
30	20	36	0,363970	Right	5,87	117	19,93	11,96	75,00	47

h (cm)	h with factor (cm)	n (s/cm^1/3)	n with factor (s/cm^1/3)	Average n	Average n with factor		h (m)	h with factor (m)	n (s/m^1/3)	n with factor (s/m^1/3)	Average n	Average n with factor
0,39812	0,66353											
0,61716	1,02860											

0,58524	0,97540											
0,14089	0,23482	0,00447	0,01047				0,00141	0,00235	0,02074	0,04858		
0,24018	0,40030	0,01087	0,02546				0,00240	0,00400	0,05044	0,11818		
0,25095	0,41826	0,01169	0,02739				0,00251	0,00418	0,05427	0,12715		
0,11552	0,19254	0,00508	0,01190				0,00116	0,00193	0,02357	0,05523		
0,17976	0,29960	0,01061	0,02486	0,00805	0,01886		0,00180	0,00300	0,04926	0,11541	0,03737	0,08756
0,16135	0,26891	0,00886	0,02077				0,00161	0,00269	0,04114	0,09639		
0,10120	0,16867	0,00483	0,01131				0,00101	0,00169	0,02240	0,05248		
0,13707	0,22845	0,00800	0,01875				0,00137	0,00228	0,03714	0,08702		
0,13762	0,22936	0,00805	0,01887				0,00138	0,00229	0,03739	0,08759		
0,08020	0,13366	0,00392	0,00919				0,00080	0,00134	0,01822	0,04268		
0,09697	0,16162	0,00539	0,01262				0,00097	0,00162	0,02500	0,05857		
0,13066	0,21777	0,00885	0,02074				0,00131	0,00218	0,04109	0,09628		
0,07583	0,12639	0,00393	0,00920				0,00076	0,00126	0,01822	0,04269		
0,08770	0,14616	0,00500	0,01172	0,00608	0,01425		0,00088	0,00146	0,02321	0,05439	0,02824	0,06615
0,12793	0,21322	0,00938	0,02199				0,00128	0,00213	0,04356	0,10205		
0,06519	0,10866	0,00330	0,00774				0,00065	0,00109	0,01534	0,03593		
0,10093	0,16821	0,00685	0,01604				0,00101	0,00168	0,03178	0,07445		
0,11184	0,18640	0,00812	0,01903				0,00112	0,00186	0,03771	0,08834		
0,06369	0,10616	0,00341	0,00799				0,00064	0,00106	0,01582	0,03707		
0,09656	0,16094	0,00682	0,01598				0,00097	0,00161	0,03166	0,07417		
0,10979	0,18299	0,00845	0,01979				0,00110	0,00183	0,03921	0,09187		
0,06833	0,11388	0,00408	0,00956	0,00652	0,01527		0,00068	0,00114	0,01894	0,04436	0,03025	0,07086
0,09875	0,16458	0,00754	0,01765				0,00099	0,00165	0,03498	0,08195		
0,10843	0,18071	0,00881	0,02063				0,00108	0,00181	0,04088	0,09577		
0,06083	0,10138	0,00356	0,00833				0,00061	0,00101	0,01651	0,03868		
0,07733	0,12889	0,00531	0,01243	0,00483	0,01131		0,00077	0,00129	0,02463	0,05771	0,02241	0,05251
0,08006	0,13343	0,00562	0,01317				0,00080	0,00133	0,02610	0,06114		

Annex 1.3. Experiment 3

Nr	Angle (°)	Slope (%)	Slope (-)	Dye position	Time (s)	Length (cm)	Velocity (cm/s)	Velocity with factor (cm/s)	Inflow (cm^3/s)	b (cm)
1	0	0	0,000000	Left	26,48	117	4,42	2,65	58,33	47
2	0	0	0,000000	Middle	67,08	117	1,74	1,05	58,33	47
3	0	0	0,000000	Right	59,5	117	1,97	1,18	58,33	47
4	2	3	0,034921	Left	14,75	117	7,93	4,76	58,33	47
5	2	3	0,034921	Middle	16,54	117	7,07	4,24	58,33	47
6	2	3	0,034921	Right	13,48	117	8,68	5,21	58,33	47
7	5	9	0,087489	Left	8,87	117	13,19	7,91	58,33	47
8	5	9	0,087489	Middle	14,82	117	7,89	4,74	58,33	47
9	5	9	0,087489	Right	11,49	117	10,18	6,11	58,33	47
10	7	12	0,122785	Left	7,98	117	14,66	8,80	58,33	47
11	7	12	0,122785	Middle	10,52	117	11,12	6,67	58,33	47
12	7	12	0,122785	Right	9,74	117	12,01	7,21	58,33	47
13	10	18	0,176327	Left	6,59	117	17,75	10,65	58,33	47
14	10	18	0,176327	Middle	8,65	117	13,53	8,12	58,33	47
15	10	18	0,176327	Right	8,67	117	13,49	8,10	58,33	47
16	12	21	0,212557	Left	6,87	117	17,03	10,22	58,33	47
17	12	21	0,212557	Middle	7,7	117	15,19	9,12	58,33	47
18	12	21	0,212557	Right	8,43	117	13,88	8,33	58,33	47
19	14	25	0,249328	Left	6,45	117	18,14	10,88	58,33	47
20	14	25	0,249328	Middle	7,52	117	15,56	9,34	58,33	47
21	14	25	0,249328	Right	7,76	117	15,08	9,05	58,33	47
22	16	29	0,286745	Left	5,77	117	20,28	12,17	58,33	47

23	16	29	0,286745	Middle	7,16	117	16,34	9,80	58,33	47
24	16	29	0,286745	Right	8,01	117	14,61	8,76	58,33	47
25	18	32	0,324920	Left	5,69	117	20,56	12,34	58,33	47
26	18	32	0,324920	Middle	6,9	117	16,96	10,17	58,33	47
27	18	32	0,324920	Right	7,83	117	14,94	8,97	58,33	47
28	20	36	0,363970	Left	5,66	117	20,67	12,40	58,33	47
29	20	36	0,363970	Middle	8,93	117	13,10	7,86	58,33	47
30	20	36	0,363970	Right	7,85	117	14,90	8,94	58,33	47

h (cm)	h with factor (cm)	n (s/cm^1/3)	n with factor (s/cm^1/3)	Average n	Average n with factor		h (m)	h with factor (m)	n (s/m^1/3)	n with factor (s/m^1/3)	Average n	Average n with factor
0,28090	0,46817											
0,71158	1,18597											
0,63118	1,05196											
0,15647	0,26078	0,00684	0,01603				0,00156	0,00261	0,03175	0,07439		
0,17546	0,29243	0,00828	0,01940				0,00175	0,00292	0,03843	0,09004		
0,14300	0,23833	0,00589	0,01379				0,00143	0,00238	0,02733	0,06402		
0,09409	0,15682	0,00464	0,01087				0,00094	0,00157	0,02153	0,05045		
0,15721	0,26202	0,01091	0,02557	0,00689	0,01615		0,00157	0,00262	0,05066	0,11868	0,03199	0,07496
0,12189	0,20314	0,00714	0,01673				0,00122	0,00203	0,03314	0,07765		
0,08465	0,14109	0,00461	0,01080				0,00085	0,00141	0,02139	0,05011		
0,11160	0,18599	0,00730	0,01711				0,00112	0,00186	0,03390	0,07942		
0,10332	0,17220	0,00642	0,01505				0,00103	0,00172	0,02981	0,06985		
0,06991	0,11651	0,00401	0,00940				0,00070	0,00117	0,01863	0,04365		
0,09176	0,15293	0,00632	0,01480	0,00562	0,01316		0,00092	0,00153	0,02931	0,06868	0,02608	0,06110
0,09197	0,15329	0,00634	0,01485				0,00092	0,00153	0,02943	0,06895		
0,07288	0,12146	0,00472	0,01107				0,00073	0,00121	0,02192	0,05136		

0,08168	0,13614	0,00571	0,01338				0,00082	0,00136	0,02651	0,06212		
0,08943	0,14904	0,00664	0,01556				0,00089	0,00149	0,03083	0,07224		
0,06842	0,11404	0,00460	0,01079				0,00068	0,00114	0,02137	0,05008		
0,07977	0,13295	0,00595	0,01393				0,00080	0,00133	0,02760	0,06467		
0,08232	0,13720	0,00627	0,01468				0,00082	0,00137	0,02909	0,06815		
0,06121	0,10201	0,00410	0,00961	0,00575	0,01346		0,00061	0,00102	0,01904	0,04460	0,02667	0,06248
0,07595	0,12659	0,00588	0,01377				0,00076	0,00127	0,02728	0,06391		
0,08497	0,14162	0,00709	0,01660				0,00085	0,00142	0,03289	0,07705		
0,06036	0,10060	0,00427	0,00999				0,00060	0,00101	0,01980	0,04639		
0,07320	0,12199	0,00588	0,01378				0,00073	0,00122	0,02730	0,06397		
0,08306	0,13843	0,00726	0,01701				0,00083	0,00138	0,03371	0,07897		
0,06004	0,10007	0,00448	0,01048	0,00725	0,01700		0,00060	0,00100	0,02077	0,04866	0,03367	0,07889
0,09473	0,15788	0,00957	0,02242				0,00095	0,00158	0,04441	0,10406		
0,08327	0,13879	0,00772	0,01808				0,00083	0,00139	0,03583	0,08394		

Annex 2. Statistics of Manning Roughness n

Annex 2.1. Experiment 1

Annex 2.1.1. Velocity Graphs

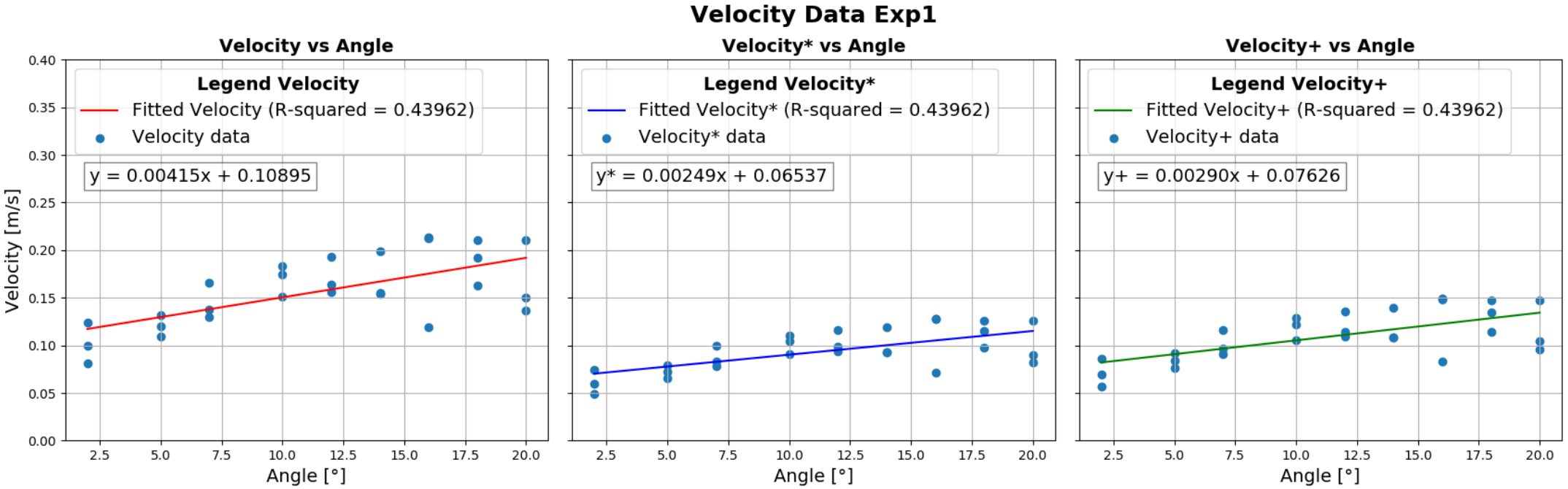

Annex 2.1.2. Water Height Graphs

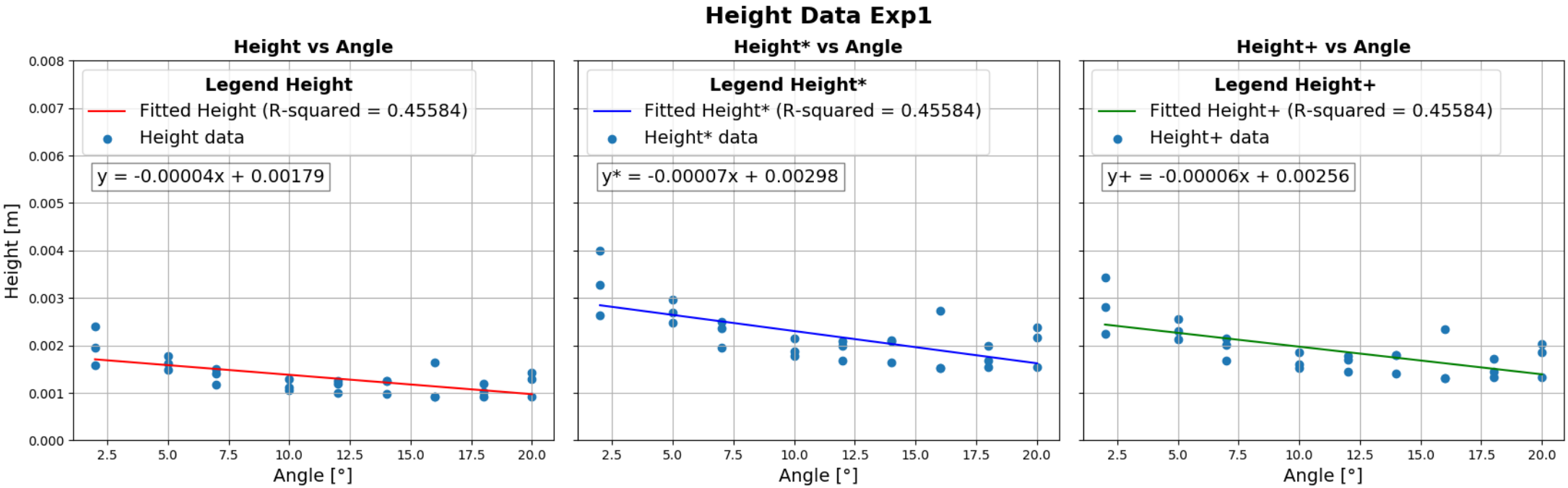

Annex 2.1.3. Manning n Statistics

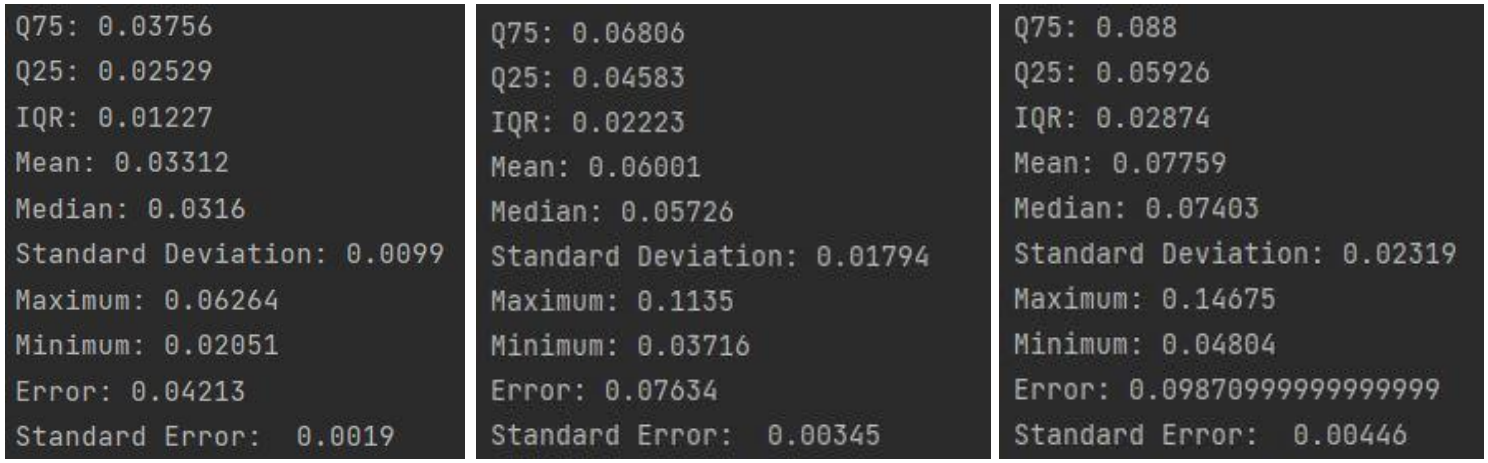

Left: no factor, middle: factor 0.7, right: factor 0.6

Annex 2.2. Experiment 2

Annex 2.2.1. Velocity Graphs

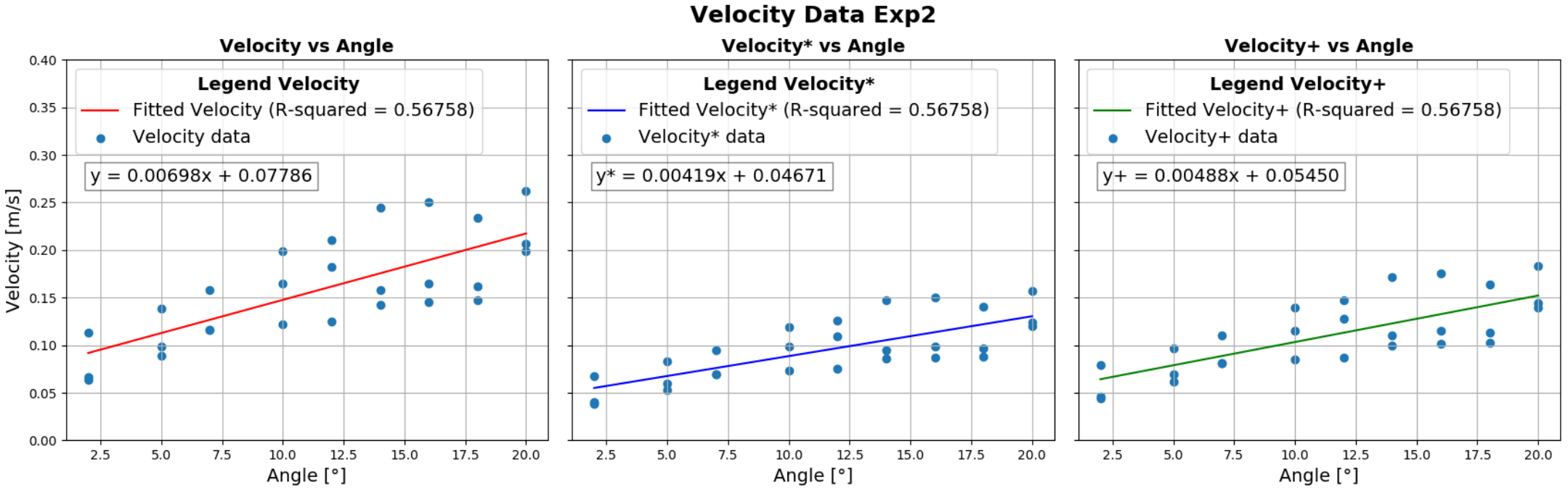

Annex 2.2.2. Water Height Graphs

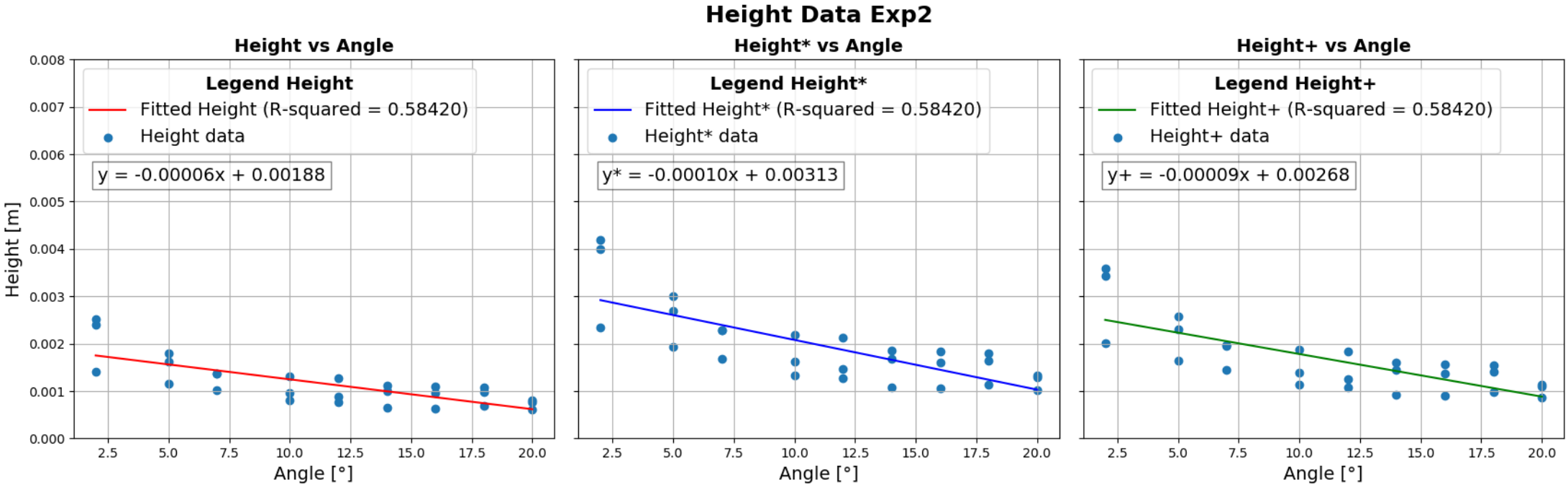

Annex 2.2.3. Manning n Statistics

```
Q75: 0.04004
Q25: 0.02157
IQR: 0.01847
Mean: 0.03108
Median: 0.03166
Standard Deviation: 0.01134
Maximum: 0.05427
Minimum: 0.01534
Error: 0.03893
Standard Error:  0.00218
```

```
Q75: 0.07256
Q25: 0.03908
IQR: 0.03348
Mean: 0.05632
Median: 0.05736
Standard Deviation: 0.02056
Maximum: 0.09834
Minimum: 0.02779
Error: 0.07055
Standard Error:  0.00396
```

```
Q75: 0.09382
Q25: 0.05053
IQR: 0.04329
Mean: 0.07282
Median: 0.07417
Standard Deviation: 0.02658
Maximum: 0.12715
Minimum: 0.03593
Error: 0.09122000000000002
Standard Error:  0.00511
```

Left: no factor, middle: factor 0.7, right: factor 0.6

Annex 2.3. Experiment 3

Annex 2.3.1. Velocity Graphs

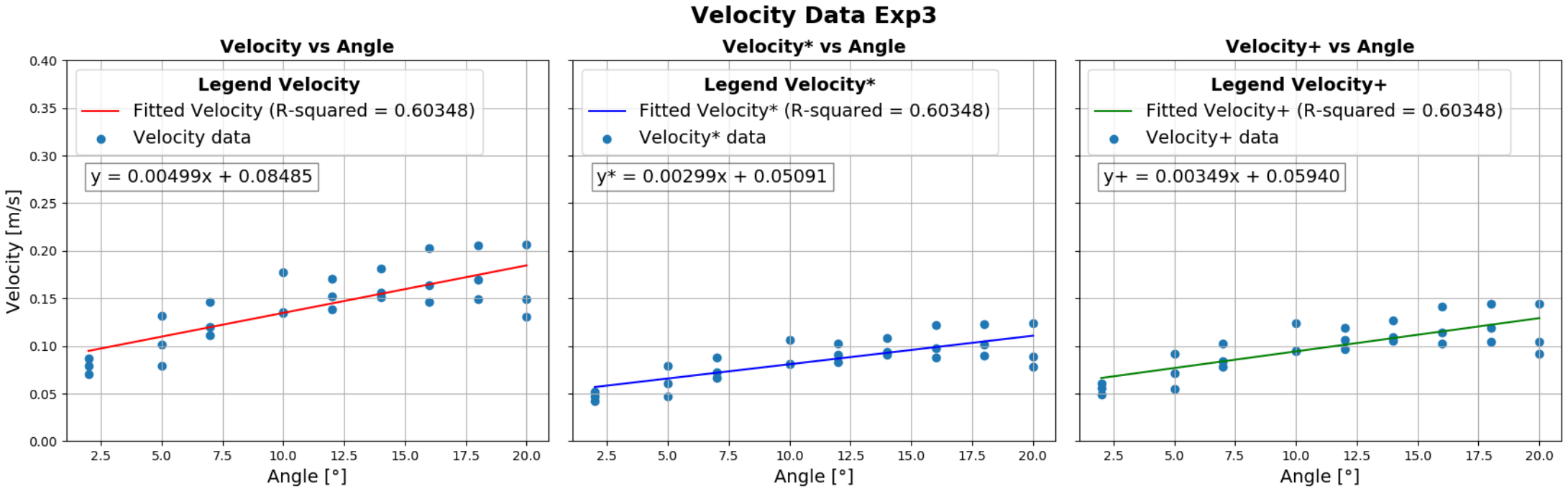

Annex 2.3.2. Water Height Graphs

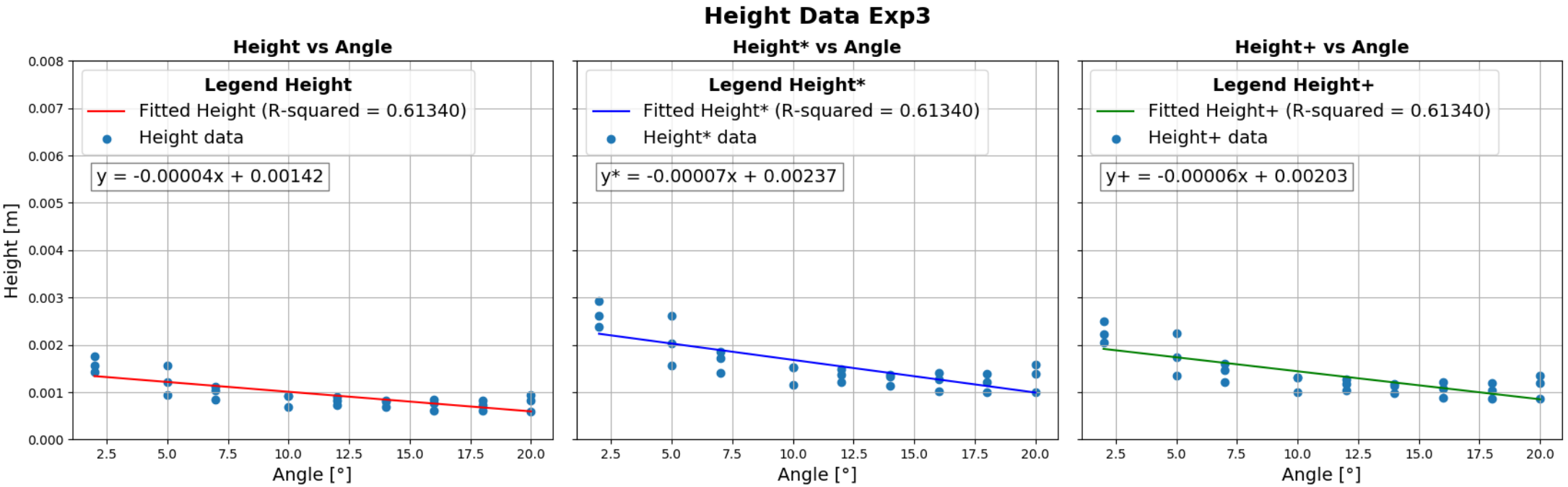

Annex 2.3.3. Manning n Statistics

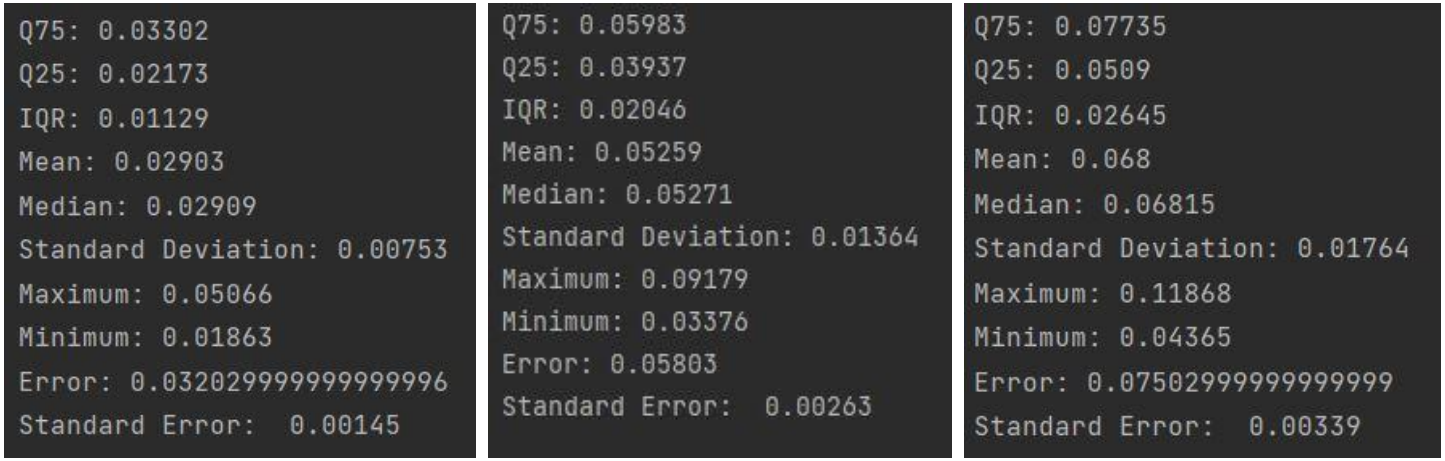

Left: no factor, middle: factor 0.7, right: factor 0.6

Annex 3. QGIS

Annex 3.1. Area 16

Annex 3.1.1. Water Depths

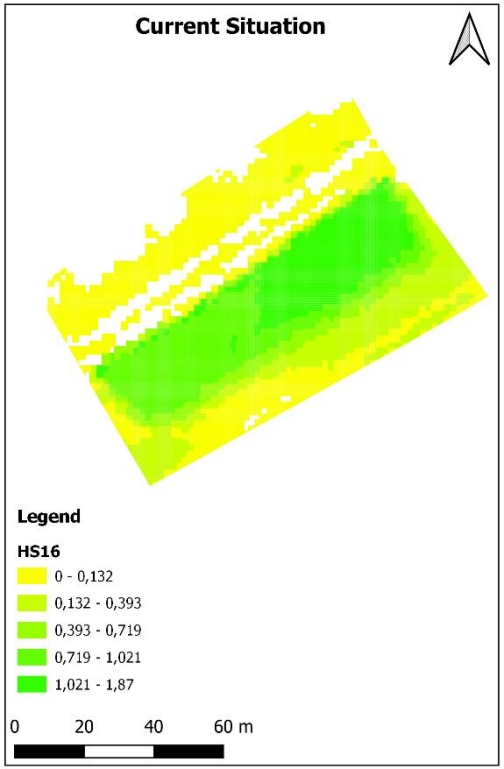

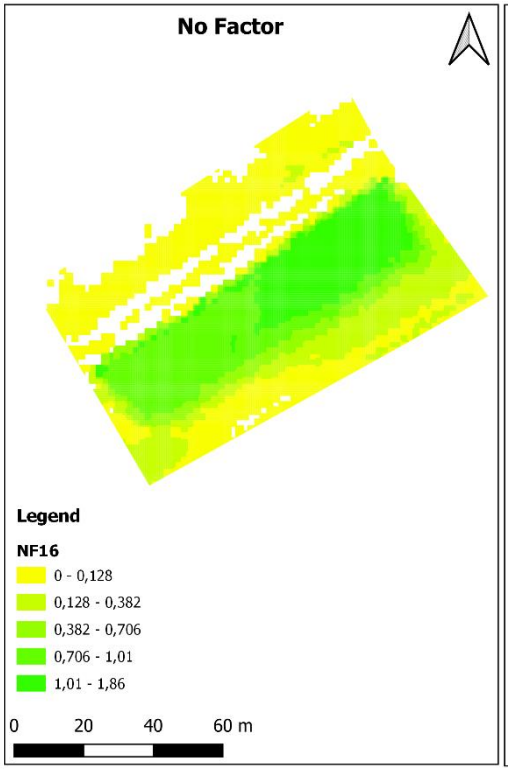

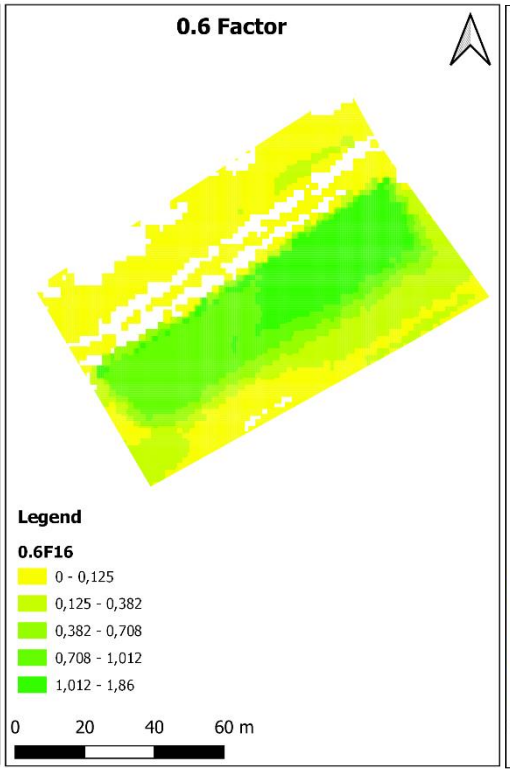

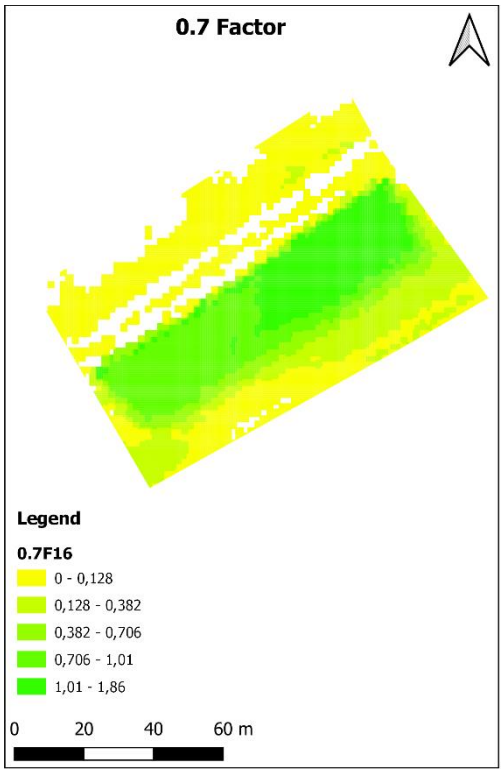

Annex 3.1.2. Difference Maps

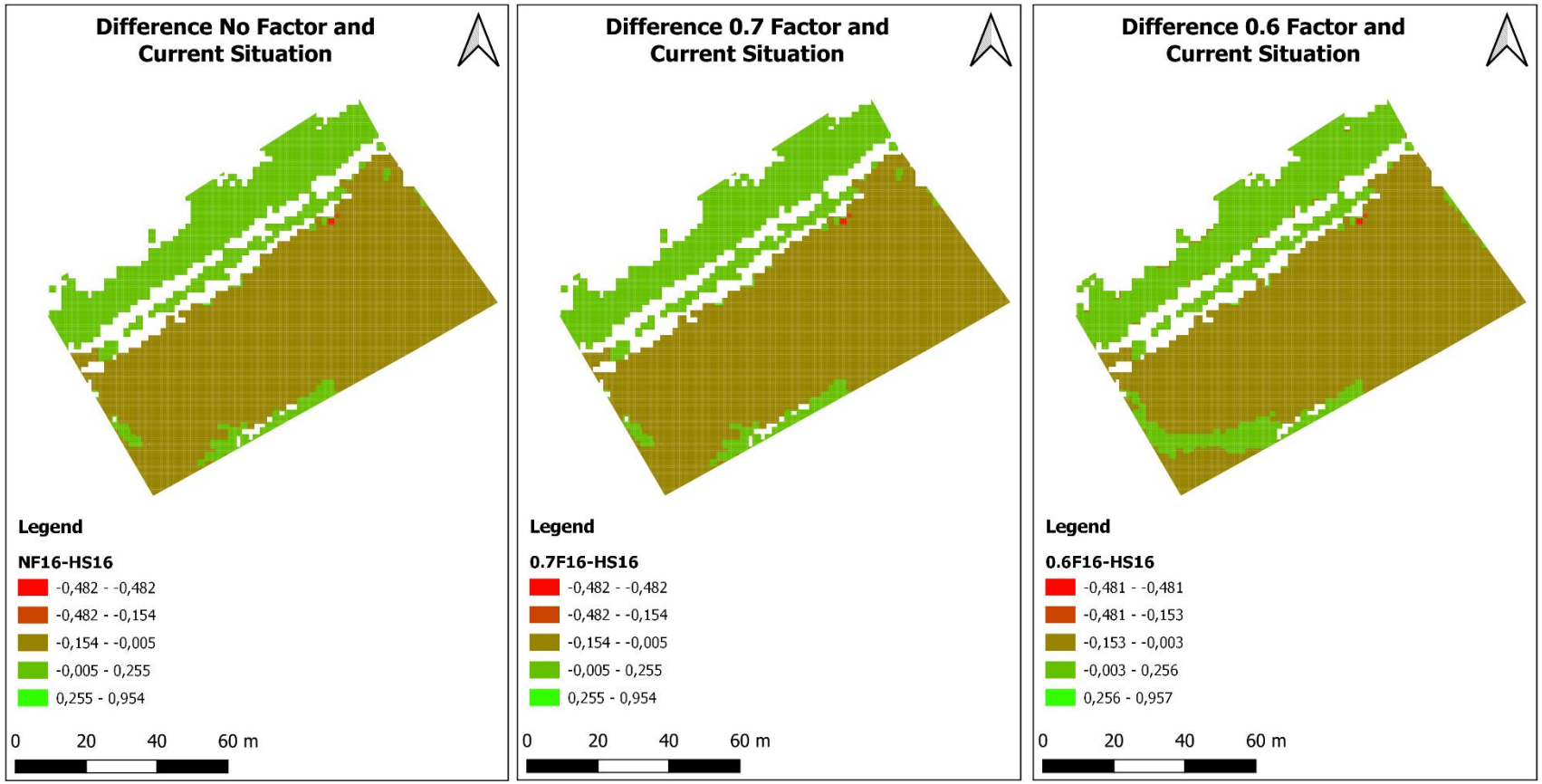

Annex 3.2. Area 18

Annex 3.2.1. Water Depths

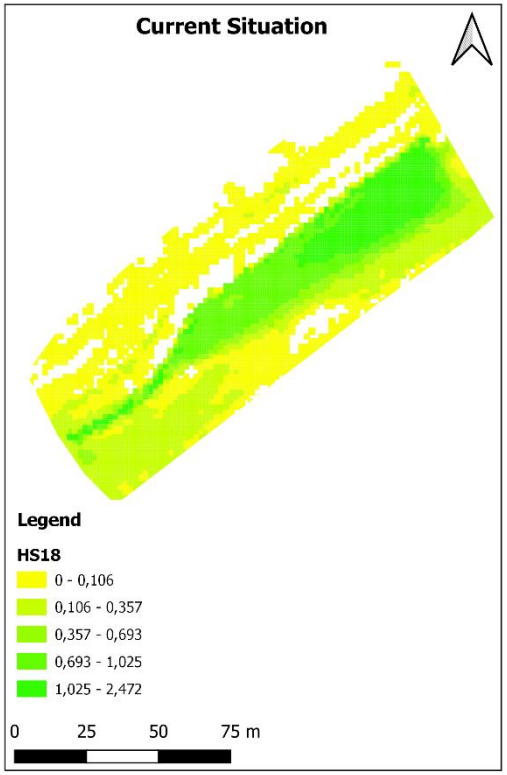

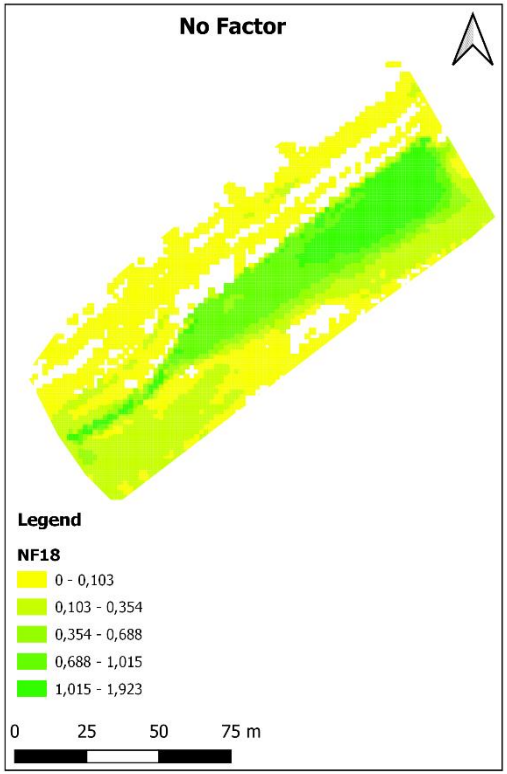

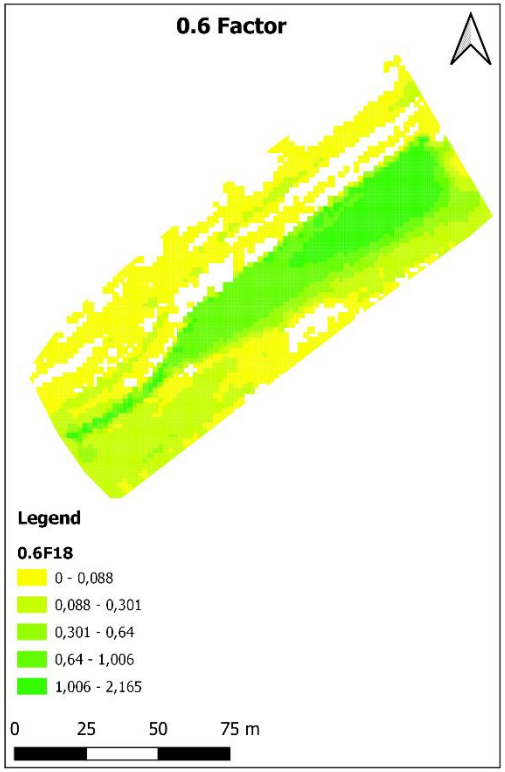

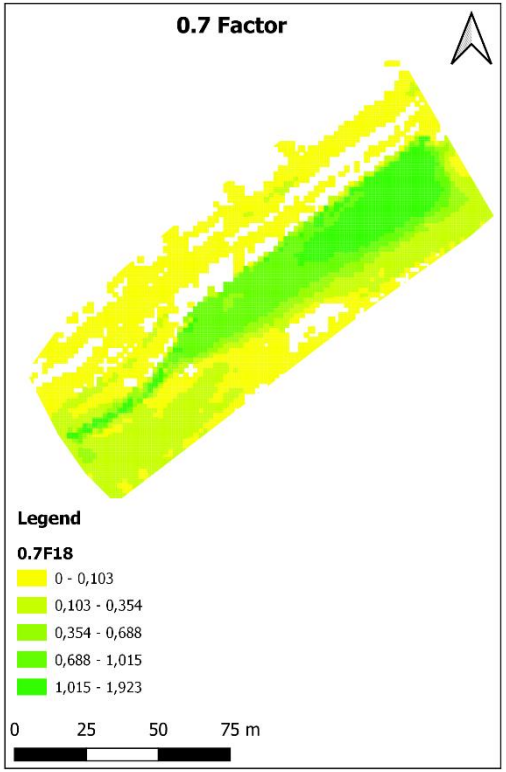

Annex 3.2.2. Difference Maps

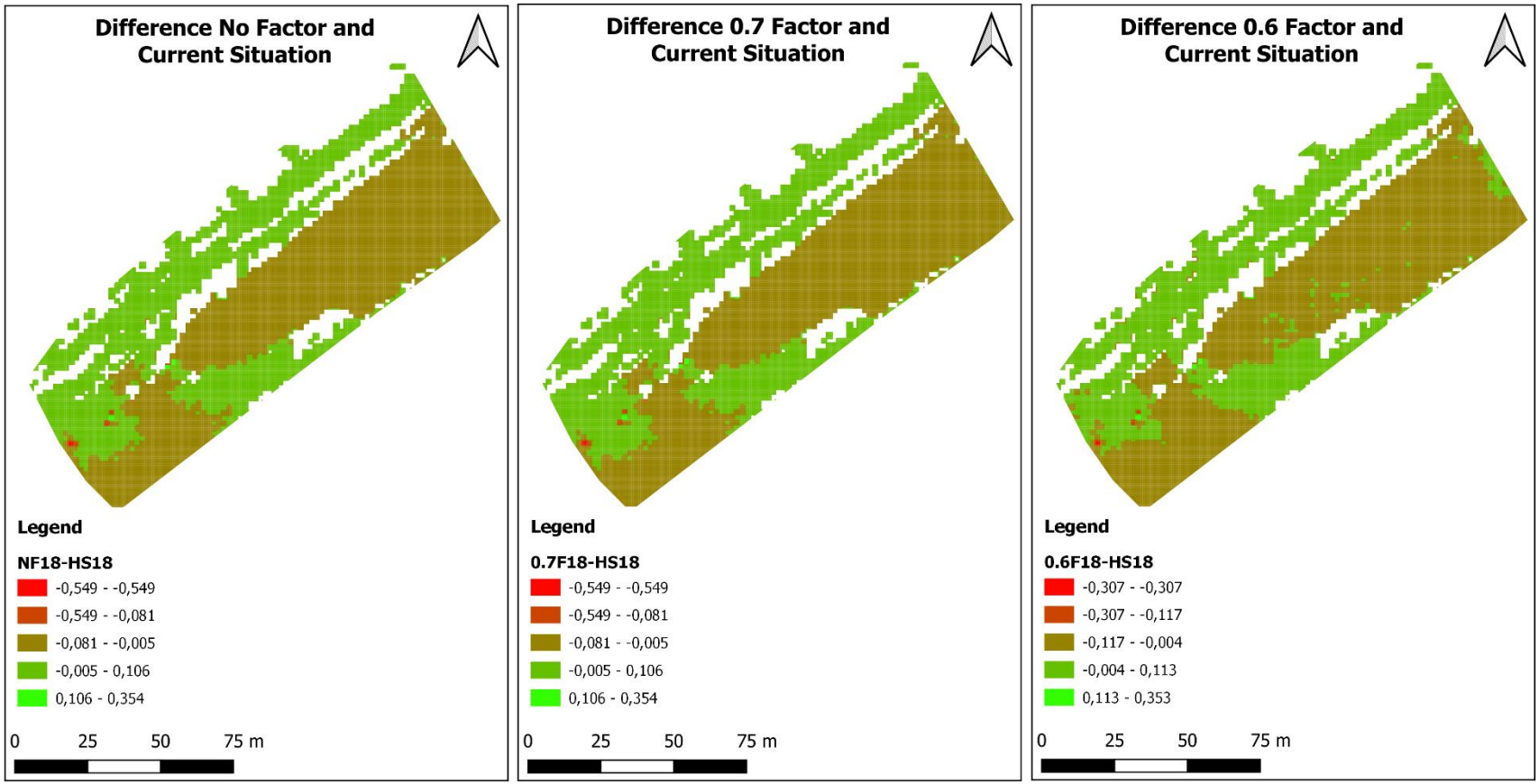

Annex 4. Histograms Manning n

Annex 4.1. Manning Roughness Coefficients Exp1

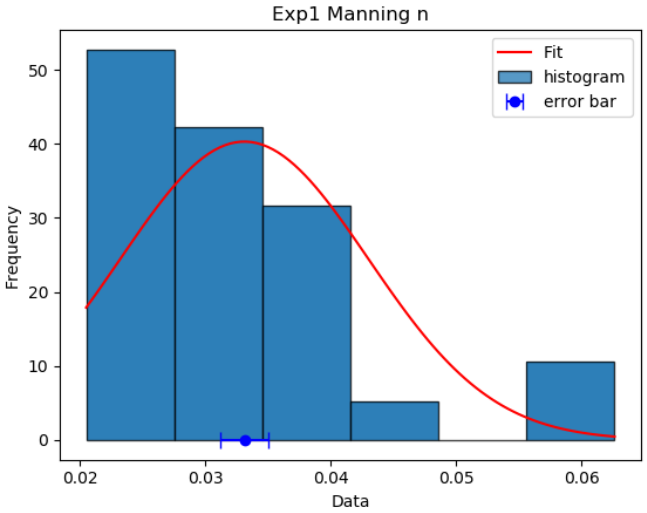

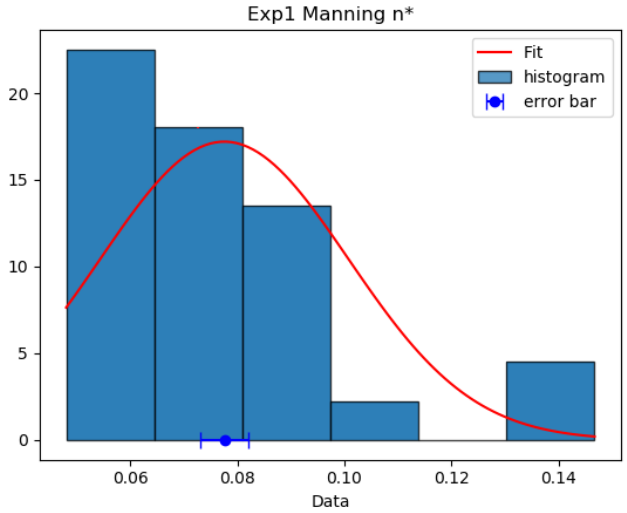

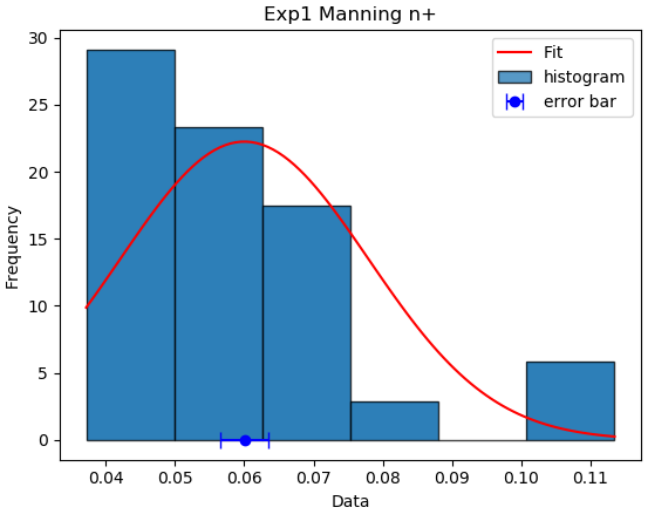

Annex 4.2. Manning Roughness Coefficients Exp2

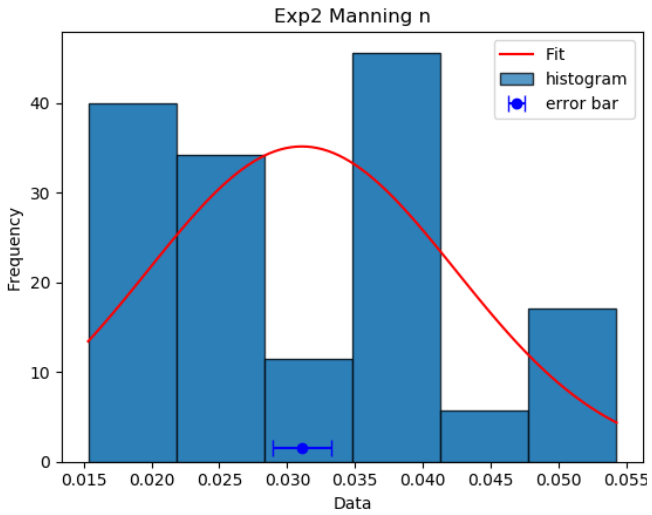

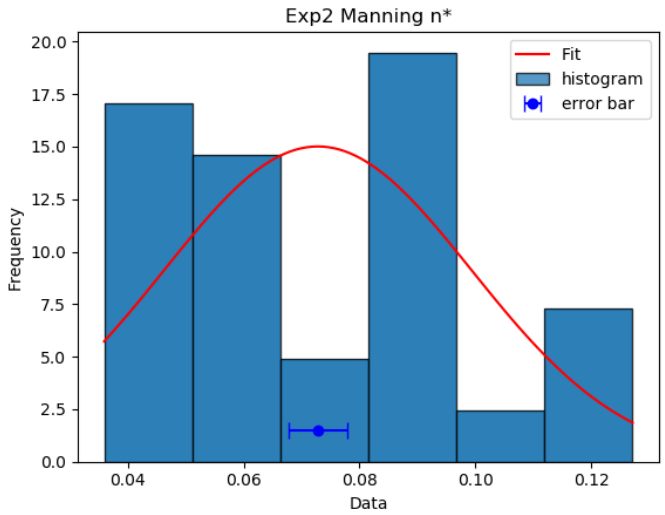

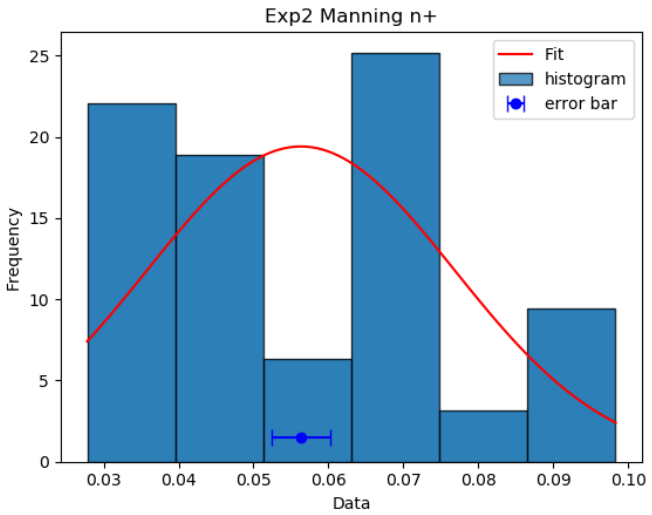

Annex 4.3. Manning Roughness Coefficients Exp3